Maria Teresa Gonçalves Lobato de Almeida

Licenciatura em Engenharia de Micro e Nanotecnologia

Radiation Damage in Flexible TFTs and Organic Detectors

Dissertação para obtenção do Grau de Mestre em
Engenharia de Micro e Nanotecnologia

Orientador: Doutor Tobias Cramer, Investigador UNIBO, Dipartimento di Fisica e Astronomia, Università di Bologna.
Co-orientador: Doutor Pedro Barquinha, Professor Auxiliar, Faculdade de Ciências e Tecnologias, Universidade Nova de Lisboa.

Júri:

Presidente: Prof. Doutor Rodrigo Ferrão de Paiva Martins
Arguente: Prof. Doutora Joana Maria Doria Vaz Pinto
Vogal: Prof. Doutor Pedro Miguel Cândido Barquinha

FCt FACULDADE DE
CIÊNCIAS E TECNOLOGIA
UNIVERSIDADE NOVA DE LISBOA

September de 2015

Radiation Damage in Flexible TFTs and Organic Detectors

Acknowledgments

This work would not have been possible without the help, care and support of some people, which could not fail to express my sincere thanks.

First, I would like to express my gratitude to Professor Rodrigo Martins and Professor Elvira Fortunato for the opportunity and support for the concretization of this thesis.

To Professor Beatrice Fraboni, a sincerely thanks for all the advices and support.

I would like to thank to my supervisors:

In particular to Doctor Tobias Cramer, I appreciate the support, sharing of knowledge and the valuable contributions given.

To Professor Pedro Barquinha for all the advices and being there when I needed.

An indescribable thanks for the care, friendship and assistance to Doctor Laura Basiricò, Doctor Isacco Gualandi, Doctor Martina Perani, Doctor Andrea Ciavatti, Giacamo Rossi, Marco Calizzi and to the "Best" Marco Marzocchi.

Also, I would like to thanks to my colleagues for this 5 years, especially to João Jacinto and Susana Oliveira.

I owe a huge thanks to all my friends for the great friendship, patience and good moments passed, namely Doctor Catarina Quaresma and Raquel Machado. Even, a special thanks to Pedro Afonso for everything.

To all my family, thank you for everything, particularly my grandmother Silvina, without whom I would not have achieved what I have today.

Abstract

In this thesis was investigated the radiation hardness of the building blocks of a future flexible X-ray sensor system. The characterized building blocks for the pixel addressing and signal amplification electronics are high mobility semiconducting oxide transistors (HMSO-TFTs) and organic transistors (OTFTs), whereas the photonic detection system is based on organic semiconducting single crystals (OSSCs). TFT parameters such as mobility, threshold voltage and subthreshold slope were measured as function of cumulative X-ray dose. Instead for OSSCs conductivity and X-ray sensitivity were analysed after various radiation steps. The results show that ionizing radiation does not lead to degradation in HMSO-TFTs. Instead OTFTs show instability in mobility which is reduced up to 73% for doses of 1 kGy. OSSC demonstrate stable detector properties for the tested total dose range. As conclusion, HMSO-TFTs and OSSCs can be readily employed in the X-ray detector system allowing operation for total doses exceeding 1 kGy of ionizing radiation.

Key words: X-rays, OSSCs, HMSO-TFTs, OTFTs, radiation hardness

Resumo

Nesta tese foi investigada a resistência à radiação de todas as partes do futuro sensor flexível de raios-X. Os blocos de construção caracterizados para o endereçamento do pixel e amplificação do sinal são transístores de óxido semicondutor de alta mobilidade (HMSO-TFTs) e transístores orgânicos (OTFTs), enquanto o sistema de deteção é baseado em monocristais semicondutores orgânicos (OSSCs). As propriedades dos TFTs, tais como a mobilidade, tensão de abertura do canal e declive na região de *subthreshold* foram medidas em função da dose cumulativa de raios-X. Relativamente aos OSSCs, analisou-se a morfologia, condutividade e sensibilidade aos raios-X após a aplicação de várias doses. Os resultados indicam que a radiação não leva à degradação nos HMSO-TFTs. Pelo contrário, os OTFTs demonstram instabilidade, uma vez que a sua mobilidade tem uma redução de 73%, com doses de 1 kGy. Os OSSCs demonstraram ser estáveis para o intervalo de doses a que foram testados. Conclui-se que os HMSO-TFTs e os OSSCs podem ser facilmente empregues no sistema detetor de raios-X, permitindo a operação para doses totais superiores a 1 kGy de radiação ionizante.

Palavras-chave: raios-X, OSSCs, HMSO-TFTs, OTFTs, resistência à radiação-X

x

Acronyms

CEA – Commissariat à l´énergie atomique et aux énergies alternatives, France

CEMOP – Center of Excellence in Microelectronics Optoelectronics and Processes, Portugal

CYTOP – Fluoropolymer

DNN – 1,5-dinitronaphtalene

4HCB – 4-hydroxycyanobenzene

HMSO-TFTs – High mobility semiconductor-oxide thin film transistors

MOS – Metal - Oxide - Semiconductor

NTI – 1,8-naphthalimide

OSSCs – Organic Semiconducting Single Crystals

OTFTs – Organic thin film transistors

RFID – Radio-frequency identification

RMS – Root mean square

TFTs – Thin Film Transistors

TIPS-pentacene - 6,13-bis(triisopropylsilylethynyl)pentacene

UNICA – University of Cagliari, Italy

UNINOVA – Instituto de Desenvolvimento de Novas Tecnologias, Portugal

UNITS – University of Trieste, Italy

Symbols

C_i – Capacity of the oxide

I_{DS} – Drain-to-Source current

I_{ON}/I_{OFF} – On/Off ratio

K_α – Absorption coefficient in L shells of atomic orbital

K_β – Absorption coefficient in M shells of atomic orbital

μ – Mobility

N_t – Interface trap density

SS – Subthreshold voltage

S – Sensitivity

T_A – Annealing temperature

V_{ON} – Turn-On voltage

V_{GS} – Voltage gate-source

V_{DS} – Voltage drain-source

V_{th} – Threshold voltage

Table of Contents

List of Figures

List of Tables

Objective and thesis structure

The main goal of this work was to assess the radiation hardness of the building blocks of a direct X-ray sensor, to study how the oxide and organic TFTs performance for the pixel and readout circuitry vary with the radiation doses applied and to investigate the main degradation causes on our devices with cumulative radiation dose. Further, the impact of X-ray exposure on TIPS-pentacene single crystal detectors was studied. The work presented here is made within the framework of the FP7 European project i-Flexis, where all these components are being investigated and integrated in a flexible X-ray sensing platform.

This dissertation is organized as follow:

- Chapter 1 provides a brief introduction on X-ray detectors and the chosen materials for the tested building blocks, and on the ionizing radiation induced mechanisms on electronic devices.

- Chapter 2 contain details about the samples tested and describe the protocols used to assess the radiation hardness of the main building blocks.

- Chapter 3 is divided in two parts, one corresponding to the thin-film transistors (TFTs) and the other to the organic semiconducting crystals. It is reported the experimental results obtained from the electrical characterization and X-ray irradiation on the devices.

- Finally, chapter 4 presents the conclusions and future perspectives arising of sensor parts tested.

Chapter 1 Introduction

1.1 Motivation

Ionizing radiation detectors constitute a very important area of research due to its vast applications, such as medical imaging and diagnostics, civil security and astrophysics. The fact that electronic materials have to operate in radiation harsh environments and survive to accumulation dose during its operation life-time leads to a great attention for research on semiconductor and related detector radiation hardness.

In recent years material science has developed new material platforms for flexible and printable electronics, such as acene derivatives, semiconductors based in poly(triarylamine) (PTAA) used in thick film for diode structures [1]. Currently these materials are being tested in a new generation of direct X-ray sensors which combine properties such as flexibility, room-temperature operation, low-cost, low weight, low power consumption and can be employed in real-time imaging [2].

Detectors employ an amplifying unit coupled with a sensor unit. An innovative direct flexible X-ray detector, relaying on printable building blocks to achieve low-cost, is proposed by the iFlexis project. In particular OSSCs are proposed as the photodetectors whereas the pixel switch and the amplifying circuits employ flexible TFTs, either based on organic or oxide semiconductors. This new sensor system arises from the need for alternatives to the detectors so far proposed, which are expensive, rigid, exhibit high power consumption and cannot be applied to large areas. Hence, the combination of emerging material technologies in a single device, offering a number of attractive features, is a strong demand to achieve [2]–[4].

1.2 X-ray detectors, OSSCs and (in) organic TFTs

Detection of X-ray radiation is based on two types of detector technologies: indirect detectors and direct detectors. First technology requires two steps, needs a scintillator that converts X-rays into visible light, and a photodiode, which detects visible light and converts it in an electrical signal. The second technology is a more efficient process by converting directly ionizing radiation into an electrical signal. In fact signal-to-noise ratio is improved and there are less losses of information, since the conversion process happens within the same material, not being necessary to employ more than one device [4][5][6]. **Figure 1.1** shows a schematic about these two process of detection. Direct detectors so far commercially available are based on inorganic semiconductors, and just recently few papers reported the use of organic semiconductors as direct detectors [7][8]. However, no inexpensive and large area detectors are available. Inorganic ones, such as silicon (Si), besides exhibiting good radiation hardness, are expensive, heavy and require high power consumption. To overcome these drawbacks, OSSCs are a new sensing system proposed, able to detect directly ionizing radiation [4][5][6].
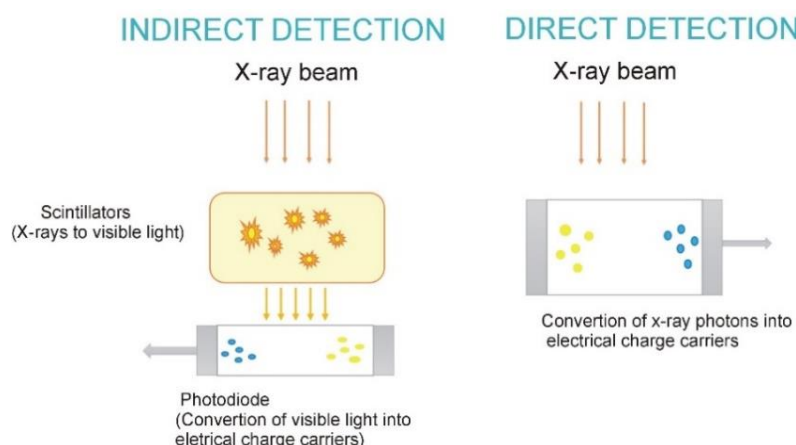
Figure 1.1 – Schematic representation of (a) indirect detection and (b) direct detection.

OSSCs are a particular class of organic semiconductors. The first investigation in organic materials started with the photoconductivity induced by x-rays and gamma-rays in the 1950s [9], and these materials were suggested for radiation detection for the first time in 1980s [10]. Recently, *Fabroni et al.*[5] reported that the OSSCs made of 4-hydroxycyanobenzene (4HCB) are able to convert directly X-ray radiation providing a fast response applying 400 V, recording a sensitivity of 50 nC/Gy, with notable radiation hardness and being able to recover after 1 month. OSSCs based on 1,8-naphthalimide (NTI) or 1,5-dinitronaphtalene (DNN), were indicated as promising solution-grown direct and active sensing system, reaching up about 6 nC/Gy applying 50V [2][4]. Even rubrene OSSCs were propose for direct ionizing radiation detection [11]. In this work 6,13-bis(triisopropylsilylethynyl)pentacene (TIPS-pentacene) crystals are studied as the active element of the sensor. TIPS-pentacene is a derivative of pentacene and it is widely used in organic electronics [12]–[14]. Attaching alkyl side chains to the backbone chains increase the molecule solubility for organic solutions, since these groups improves the π-orbital coupling intermolecular interactions leading to high mobilities in single crystals form [3][15]. In **Figure 1.2** is shown a schematic of the pentacene and TIPS-pentacene molecules.
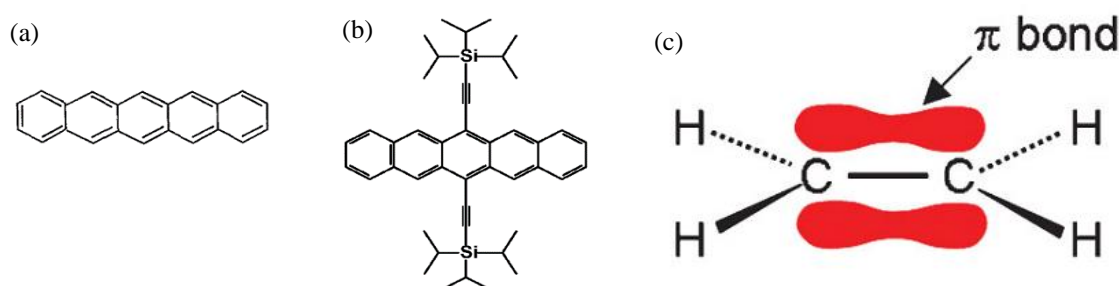
Figure 1.2 – Schematic representation of: (a) pentacene; (b) TIPS-pentacene; (c) π-bond in a conjugated organic material [3][15].

Dark current, sensitivity, response time are some of the important parameters to evaluate the performance of a photodetector. A schematic of a typical OSSC photoresponse is illustrated in **Figure 1.3** [16][17]. To achieve high sensitivity in OSSCs, the material requirements consist in a

high crystal purity, defect-free structure ensuring good charge transport, and high resistivity ($>10^9 \Omega$cm). Besides this, OSSCs should have a small band gap (<5eV) to guarantee a high electron-hole pairs generation but higher than 1.5 eV to have a low dark current ($<10^{-7}$A). Also, it is necessary to maximize the number of incident photons with a higher detector volume as possible for efficient radiation–atomic interactions. Highly efficient detection is possible by a combination of the required properties described above [2][4].

(a)   (b)
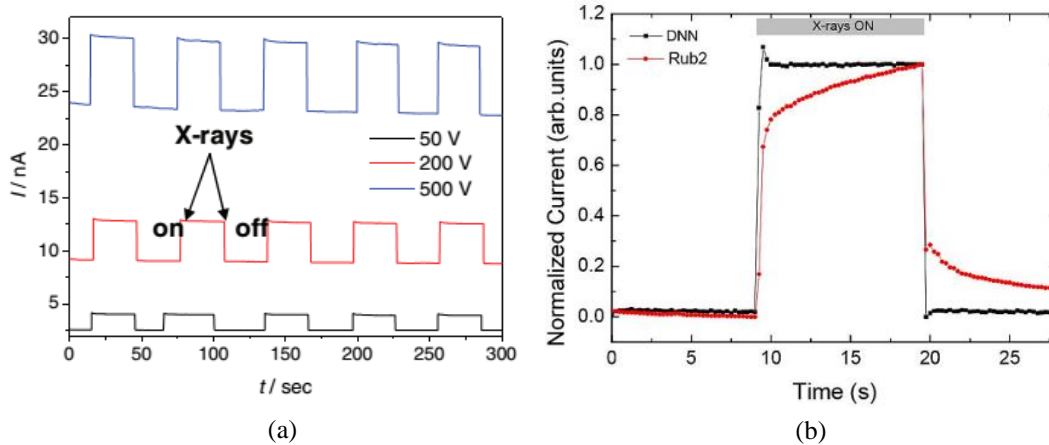
Figure 1.3 – (a) Dynamic electrical response to x-rays, with repeated ON-OFF switching, of 4HCB crystal, shown for different applied bias voltages; (b) Rubrene and DNN photoresponse biased at 50V [5][11].

In contrast to inorganic materials that rely on covalent or ionic bonds, organic semiconductors are bonded by the weak van der Waals forces. These weak forces and the resulting elastic modulus are the reason for their suitable flexibility, lightweight in organic electronics and allows them to be fabricated by printing technology or roll-to-roll process maintaining their functionality [18]. Organic semiconductors can be fabricated by solution growth [19], inkjet printing [20] and microcontact printing [21]. Their operation is related with molecular packing, purity, crystallinity, and its growth, which is an extremely important condition to achieve best performance [18].

In the platform envisaged in the i-Flexis project, the amplifying unit uses TFTs as a switch of the pixel and readout circuitry. TFTs have three electrodes, gate, source and drain, and it consists in a semiconductor layer, between the source and drain, and an insulator layer (dielectric), between gate and semiconductor layer. Basically, TFTs operate as a voltage-controlled current source. In other words, a gate–source voltage (V_{GS}) gives rise to the accumulation of electronic charges in the semiconductor, close to the semiconductor/dielectric interface. The current that flows through the semiconductor, between the source and the drain (I_{DS}), is modulated by adjusting the gate voltage. This modulation is known as field-effect [3][22].

Two promising semiconductor technologies can be considered for flexible TFTs: organics and oxides. Organic semiconductors were intensively studied from the 1980s and a great appeal for organic electronics raised, thanks to properties such as low temperature fabrication and mechanical flexibility, leading to a variety of applications as shown in **Figure 1.4**.

(a)　　　　　　　　　　　(b)　　　　　　　　　　　(c)

Figure 1.4 – Few promising organic electronics applications: (a) flexible active matrix organic light-emitting diode (AMOLED) [23]; (b) organic and flexible TFTs [24]; (c) Sensors based on organic material [25].

Best performing organic TFTs (OTFTs) are typically p-type, with mobilities ≈1 cm^2 V^{-1} s^{-1} being usually reported. Still, hole and electron mobility of 40 and 11 cm^2 V^{-1} s^{-1}, respectively, were already reported for OTFTs [26]. An interesting review on OTFTs was reported by *Klauk* [15]. On the other hand, most oxide TFTs are n-type, consistently exhibiting mobilities above 10 cm^2 V^{-1} s^{-1}, coupled with low temperature processing. Gallium-Indium-Zinc-Oxide (GIZO) and Zinc-Thin-Oxide (ZTO) are two semiconductors intensively studied for oxide TFTs [27]–[29]. One advantage of ZTO in relation to GIZO is to be indium-free, as such, is a more sustainable material to work with [30]. Dielectrics are fundamental components of any TFT technology. A comparative study between silicon dioxide dielectric and a high-k dielectric based on tantalum pentoxide and silicon dioxide (Ta_2O_5-SiO_2) was reported by *Barquinha et al.,* revealing the advantages of high-κ materials to improve overall device performance without affecting processing temperature [31]. These two dielectrics were selected for the oxide TFTs examined in this work. While, for OTFTs the organic dielectric used was the amorphous fluoropolymer (Cytop), studied in different devices by *Kalb et al.*[32].

1.3   X-ray Radiation

The X-ray tube is the most common source used to convert electron kinetic energy into X-ray radiation. An electron beam is emitted by a cathode (a filament heated), from where the electrons are accelerated by a high voltage applied (>$20kV$) toward the metal target, normally made of tungsten, copper or molybdenum. The tube is connected to a generator and has a shutter which allows the on-off switching of X-rays. The resulting interaction between the accelerated electrons and the target atoms leads to production of X-rays, due to the relaxation process after the excitation in the inner shells to the outer shells of the individual atoms. Two kinds of relaxation processes are distinguished which lead to two kinds of X-ray radiation: Bremsstrahlung X-ray and characteristic X-ray photons. In the Bremsstrahlung process, X-ray photons are emitted by the deceleration of free electrons after its interaction with bounded atomic electrons. A continuous spectrum appears with a systematic production of X-ray by this process. Whereas characteristic X-ray photons are produced right after an empty space in inner shells of the atomic orbitals is filled. The emission of these photons are characteristic of K, L, M shells, which energy corresponds to the characteristic of the anode material. Further, an X-ray discrete spectrum rises from the X-ray characteristic emission [6][33][34].

Effects of radiation have to be taken into account due to the fact that in ionizing radiation environment the devices suffer degradation and can be damaged. Degradation regards the deterioration of electronic properties of the devices as a consequence of exposure to high doses (≥100rad=1Gy). The ionizing effects depend on the absorber dose, which can be measure by radiation per unit volume in rad or Gray (Gy), the SI unit. 1 Gy corresponds to one joule per kilogram (J/Kg) and to 100 rad. Total dose effects results from the continuous build-up of trapped charge in insulating layers or in the interface semiconductor/dielectric induced by the ionizing damage. Displacement damage and ionization damage are two basic radiation effects mechanisms in semiconductors, leading to parameters changes in detectors. Displacement damage takes place when atoms are dislocated from their lattice sites by impinging radiation, which results in a modification in the electrical properties, while ionizing damage refers to the energy absorbed by ionization in insulating layers, creating charge carriers, which diffuse or drift to other locations where they are trapped. These traps can get anneal in different times scales, depending on several parameters, such as trapped charge mobility [33]–[36].

In literature it is possible to find some works about radiation damage in transistors. *Boudry et al.* [37] investigate the radiation effects in amorphous silicon field effect transistors integrated with photodiodes and, later, the research of *Li et al.* [38], on radiation damage in polycrystalline silicon (poly-Si) TFTs indicate a good resistance to radiation for dose levels up to 1000 Gy. Regarding radiation effects in conjugated polymer, where few studies have been reported [39]–[41], all indicate degradation of organics materials due to chain-scission, crosslinking, presence of oxygen and conjugation reduction. It is noteworthy that *Lujan et al.* [42]*,* besides it differs from the intended X-ray detector, had proved that a thin and flexible X-Ray imaging sensor works, which is composed by a flat-panel GIZO TFTs and an active layer of amorphous silicon photodiodes all integrated on a polyethylene naphthalate (PEN) substrate. In order to understand the effects of the incident radiation in devices *Schwank et al.* [43] investigated these physical mechanisms. A schematic energy band diagram of a Metal-Oxide-Semiconductor (MOS) structure identifying the main processes involved in radiation response of electronic devices is illustrated in **Figure 1.5**. Initially, ionizing radiation impinges the device layers creating electrons-hole pairs as it ionizes the lattice atoms. Thereafter electrons are immediately removed from the oxide due to their high mobility and positive charges remain, despite a portion of the pairs created recombines. The positive charges can be trapped and with time, they migrate to the interface Si/SiO_2 by a mechanism called hopping transport, inducing accumulation of charges. Besides, as they reach the interface, a deep trap states formation initiate that can exist for a long time. In the absence of X-ray these interfacial hole traps may get anneal and the device returns to its original performance [36][43].
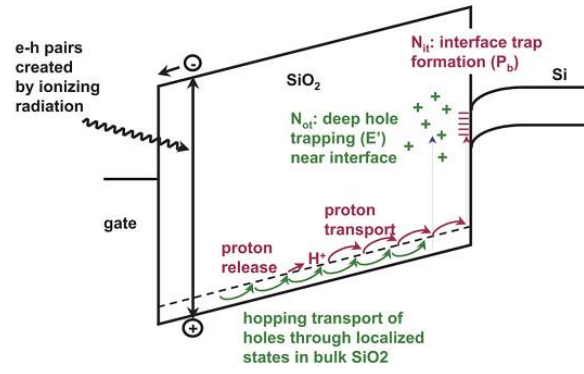
Figure 1.5 – Schematic energy band diagram for MOS structure, indicating major physical processes underlying radiation response [43].

Chapter 2 Materials and Methods

In order to assess the radiation hardness, to characterize the devices performance as a function of cumulative dose and to verify if there is any recover process, a protocol was defined. The protocol consists in subjecting the devices to ionizing radiation and characterizing their performance, as detailed in the following paragraphs.

2.1 Description of the devices

For the readout electronics the oxide TFTs samples used in this study were produced at CEMOP-UNINOVA and the organic TFTs were fabricated by CEA. Details about HMSO-TFTs fabrication are described in **Table 2.1**. Samples A and C were annealed at 200ºC for 1 hour in a hot plate after electrodes deposition and sample B was annealed at 300ºC after ZTO deposition and at 150ºC after electrode deposition. All the analysed devices had a width (W) of 80 μm and a channel length (L) of 20 μm and they are non-passivated. Fabrication processes are summarized in **Appendix 1** for HMSO-TFTs and in **Appendix 2** for OTFTs. OTFTs (W = 2000 μm; L = 50 μm), were fabricated employing screen printing technique onto a flexible substrate, with a top-gate bottom-contact structure for both N and P-type devices. Relatively to the sensor unit, UNICA has provided polycrystalline film TIPS-pentacene devices, which were composed by interdigitated gold electrodes onto a PET substrate and UNITS has fabricated TIPS-pentacene OSSCs by inkjet printing with tetralin and toluene solvents.

Table 2.1 – Matrix of HMSO-TFTs combinations and fabrication conditions at UNINOVA to assess radiation hardness at UNIBO.

	Sample A (Glass substrate)			Sample B (Si substrate)			Sample C (Glass substrate)		
	Material	**Deposition Technique**	**Thickness**	**Material**	**Deposition Technique**	**Thickness**	**Material**	**Deposition Technique**	**Thickness**
Active Layer	GIZO	Sputtering	40 nm	ZTO	Sputtering	40 nm	ZTO	Sputtering	40 nm
Dielectric	Ta_2O_5/SiO_2	Sputtering	250 nm	SiO_2	Thermal oxide	100 nm	Ta_2O_5/SiO_2	Sputtering	250 nm
Contacts	Molybdenum	Sputtering	60 nm	GAZO	Sputtering	200 nm	Molybdenum	Sputtering	60 nm

2.2 Electrical characterization and Radiation hardness

TFTs electrical characterization was carried out in air at room temperature in a probe station, micromanipulators had tungsten tips with a radius of 25 μm, integrated with a Keithley 2614 source-meter. Three current-voltage measurements (*IV*) were performed: output (sweeping V_{DS} for different V_{GS} steps), linear and saturation transfer characteristics (sweeping V_{GS} for a constant V_{DS}). In **Table 2.2** are reported the values used to perform output and transfer characteristics

measurements for oxide samples, and for OTFTs the values applied are reported in **Table 2.3**. These measurements were performed before and after each radiation dose applied.

Table 2.2 – Values used for the measurements on the samples A, B, C.

	Parameters		Linear	Saturation	Output
Samples A, C	V_{GS} (V)	Start	-5	-5	0
		Stop	5	5	5
	V_{DS} (V)	Start	0.1	10	0
		Stop			10
Sample B	V_{GS} (V)	Start	-5	-5	0
		Stop	15	15	15
	V_{DS} (V)	Start	0.1	15	0
		Stop			15

Table 2.3 – Values used on the measurements for N-type and P-type OTFTs.

		N-type		P-type		Both types
Parameters		Linear	Saturation	Linear	Saturation	Output
V_{GS} (V)	Start	-15	-15	-60	-60	20
	Stop	60	60	15	15	60
V_{DS} (V)	Start	1	60	-1	-60	-5
	Stop					60

X-ray irradiation measurements have been performed in dark, in air and at room temperature with a molybdenum X-ray tube (PANanalytical PW2285/20 tube) at 35 kV of accelerating voltage. More than 4 independent TFTs were tested to allow a significant statistical analysis. HMSO-TFTs were exposed to four consecutive radiation doses of 500 Gy each. The samples were irradiated for 70 minutes with a filament current of 30 mA providing a maximum dose rate of 117 mGy/s. Electrical measurements were performed 10 minutes after each irradiation dose. The samples were stored in dark for 13 hours after the fourth irradiation, and an electrical characterization was performed to investigate how the samples recover in the absence of X-rays. OTFTs were also characterized following the same protocol as the HMSO-TFTs, but with a maximum dose rate of 60.4 mGy/s providing 250 Gy per dose. To investigate X-ray induced degradation processes in the sensor performance in the polycrystalline film TIPS-pentacene the protocol is described in **Table 2.4**. Each irradiation was applied for 70 minutes with a dose rate of 60.4 mGy/s and after each irradiation, applying a bias of 0.2 V, the following electrical measurements were carried out: an initial current-voltage (*IV*) measurement, then six measurements (each one for a different dose rate) where the sample was biased at a constant voltage while *It* was subjected to X-rays at fixed time intervals to determine its detection sensitivity, and a final *IV* measurement with no X-rays. Instead, for TIPS-pentacene OSSCs, only the sensitivity and the X-rays photoresponse was investigated, performing an identical electrical characterization as the one used for the polycrystalline samples, but applying a bias of 1 and 5 V.

Table 2.4 – Description of each step of the protocol used on TIPS-pentacene polycrystalline film device.

Steps	Description
0	Electrical characterization
1	1st radiation dose and electrical characterization
2	2nd radiation dose and electrical characterization
3	3rd radiation dose and electrical characterization
4	4th radiation dose and electrical characterization
5	Samples rest 22h in dark and electrical characterization

Table 2.4 – Description of each step of the protocol used on TIPS-pentacene polycrystalline film device.

12

Chapter 3 Results and Discussion

As explained before, a radiation sensor has to perform well under harsh environments, therefore it is important to analyse the main degradation processes involved in the sensor parts assessing their radiation hardness and their stability in function of time and accumulative doses. In this chapter, the results from X-ray irradiation and electrical characterization experiments carried out, in both building blocks, are described and discussed.

3.1   Radiation Hardness on transistors for pixel/readout circuits.

The amplifying unit uses TFTs as switch of the pixel and readout circuitry, hence oxide and organic TFTs were tested and characterized as function of accumulative dose and time. Due to the application of the sensor it is important to characterize the degradation effects and the damage on their electrical performance exposing them to high radiation doses. Oxide and organic TFTs had received 2 kGy and 1 kGy, respectively, as the total doses applied to understand how harsh they are to the radiation. Per dose they received 500 Gy (for oxides) and 250 Gy (for organics), which is a similar dose to a mammography imager that received 250 Gy over 5 years, and in radiotherapy imaging the largest dose levels expected that can be given for an array is about 10^4 Gy cumulative dose [37][38].

3.1.1 Oxide Thin-Film Transistors

The cross-sections schemes from this set of samples are illustrated in **Figure 3.1**. The set comprises different combinations of semiconductor, dielectric and electrode films in order to select the most appropriate regarding radiation hardness. The capacitance of sample A and C is 50 nF/cm^2 and for sample B is 34 nF/cm^2. For each oxide devices tested, typical current-voltage measurements, output and transfer characteristics, are presented in **Figure 3.2**.
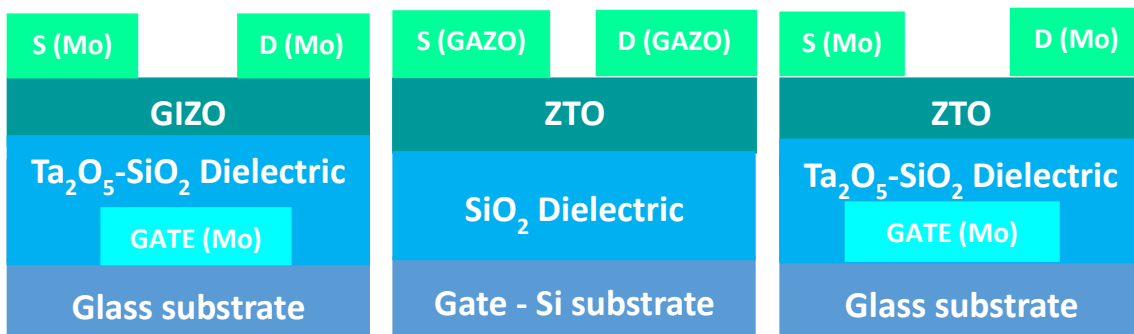
Figure 3.1 – Schematics of the oxide TFT cross-sections analysed during this project.
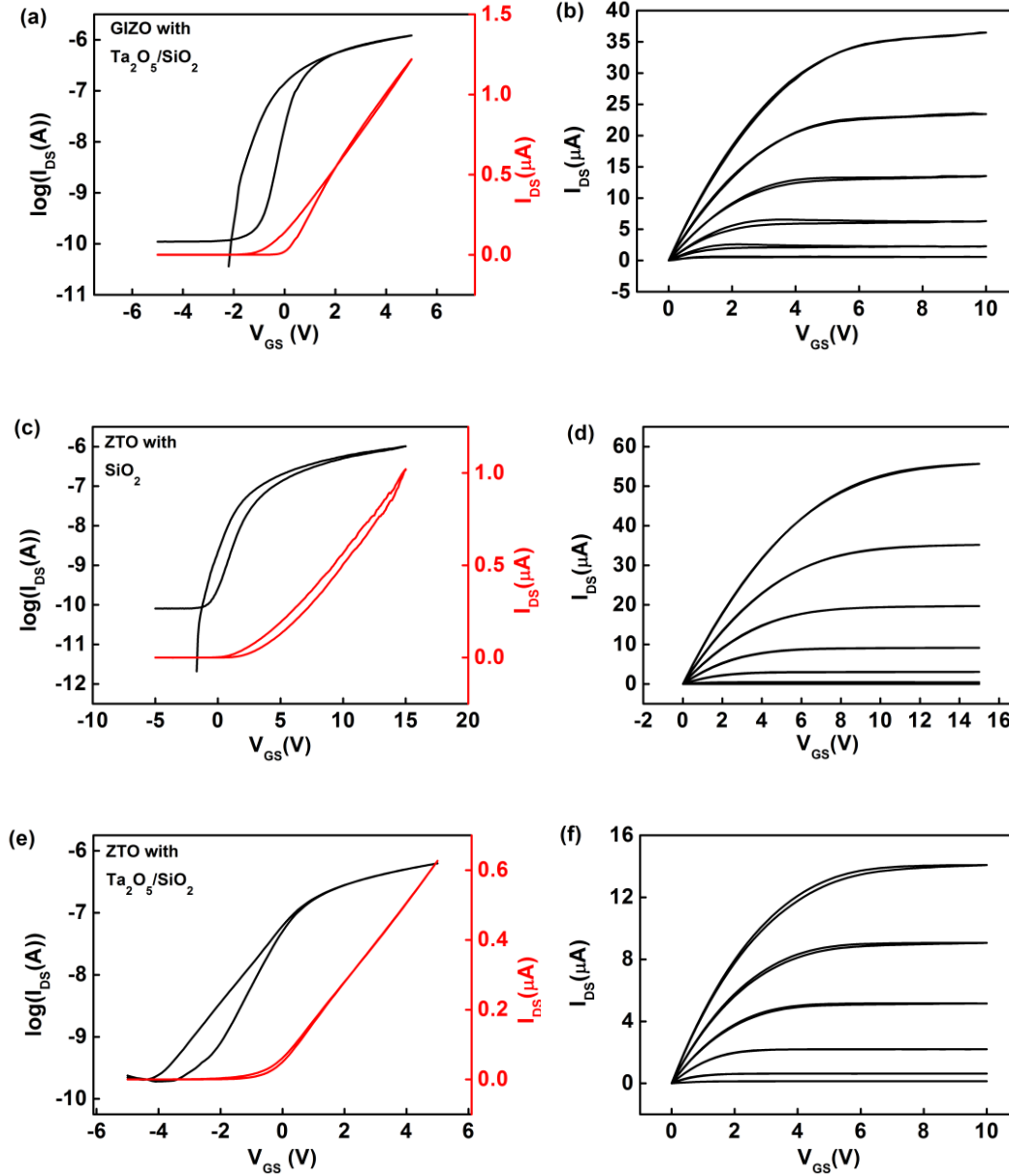
Figure 3.2 – Transfer characteristics (V_{DS} = 0.1 V) on left, with the respective output curves on right, before irradiation: (a) and (b): Sample A; (c) and (d): sample B; (e) and (f) sample C.

For all the samples clockwise hysteresis is visible in the transfer characteristics, consistent with a typical charge trapping mechanism at the dielectric/semiconductor interface. All the output curves show very close to ideal transistor behaviour, with I_{DS} scaling linearly with V_{DS}, for low V_{DS} and I_{DS} saturation for large V_{DS}. This suggests good contact properties and complete channel pinch-off, respectively. Current-voltage characteristics can be described by the following standard equations related with transistor operation, linear regime (1) and saturation regime (2):

$$I_{DS} = \frac{W}{L} \cdot \mu \cdot V_{DS} \cdot C_i \cdot (V_{GS} - V_{th}) \tag{1}$$

$$I_{DS} = \frac{1}{2} \cdot \frac{W}{L} \cdot \mu \cdot C_i \cdot (V_{GS} - V_{th})^2 \tag{2}$$

14

Linear regions of I_{DS} vs V_{GS} (for linear regime) and square root (sqrt) I_{DS} vs V_{GS} (for saturation regime) were fitted with (1) and (2) to extract mobility and threshold voltage (V_{th}). Mobility corresponds to the slope of the line, whereas V_{th} is obtained from the extrapolation of the line to zero current. From the log scale of the transfer curves were obtained others parameters, namely On/Off ratio, V_{ON} and SS. Interfacial trap density, N_t, was estimated following the equation (3) obtained from the measurement of SS:

$$SS = \frac{kT \ln 10}{e} \cdot \left[1 + \frac{e^2}{C_i} \cdot N_t \right] \tag{3}$$

Where kT is equal to 0.025 eV at room temperature, C_i is the gate capacitance per unit area and e is the elementary charge. In order to get representative data, all the results were acquired from statistical analysis, measuring more than four transistors for the same kind of sample. In **Table 3.1** is reported the average of the pristine parameters values extracted from linear transfer characteristics ($V_{DS} = 0.1$ V) with the respective Root Mean Square (RMS) values, for each device.

Table 3.1 – Electrical parameters of pristine oxide TFTs, prior to degradation tests. RMS values are presented for all parameters, calculated in linear regime ($V_{DS} = 0.1$ V).

TFT Parameter	Sample A	Sample B	Sample C
Semiconductor	GIZO	ZTO	ZTO
Dielectric	Ta_2O_5/SiO_2	SiO_2	Ta_2O5/SiO_2
Substrate	Glass	Si	Glass
μ (cm^2/Vs)	11.0 ± 2.0	6.1 ± 0.4	5.6 ± 0.5
V_{th} (V)	-0.3 ± 0.7	3.2 ± 0.2	-0.5 ± 0.4
V_{ON} (V)	-2.8 ± 0.8	-1.5 ± 0.5	-4.0 ± 1.0
$\log_{10}(I_{ON}/I_{OFF})$	5.3 ± 1.0	4.4 ± 0.1	3.7 ± 0.2
SS (V/dec)	0.41 ± 0.09	0.90 ±0.10	1.2 ± 0.2

As we can see in **Table 3.1**, mobility values reported were for ZTO around 6 $cm^2V^{-1}s^{-1}$ and for GIZO 11 $cm^2V^{-1}s^{-1}$. Higher mobilities were expected for GIZO, once it is composed by indium, which is an element reported in literature as very conductive, and so with the high mobilities. Subthreshold values reported are less than 2 V/dec. The ratio between the maximum drain current (on-state) and the minimum drain current (off-state) is about 10^4.

Later, these high mobility oxide TFTs had been irradiated up to 2 kGy and it was investigated the devices performance as the doses were applied. **Figure 3.3** shows linear transfer characteristics corresponding to the pristine measurement and all the measurements carried out for 500, 1000, 1500 and 2000 Gy.
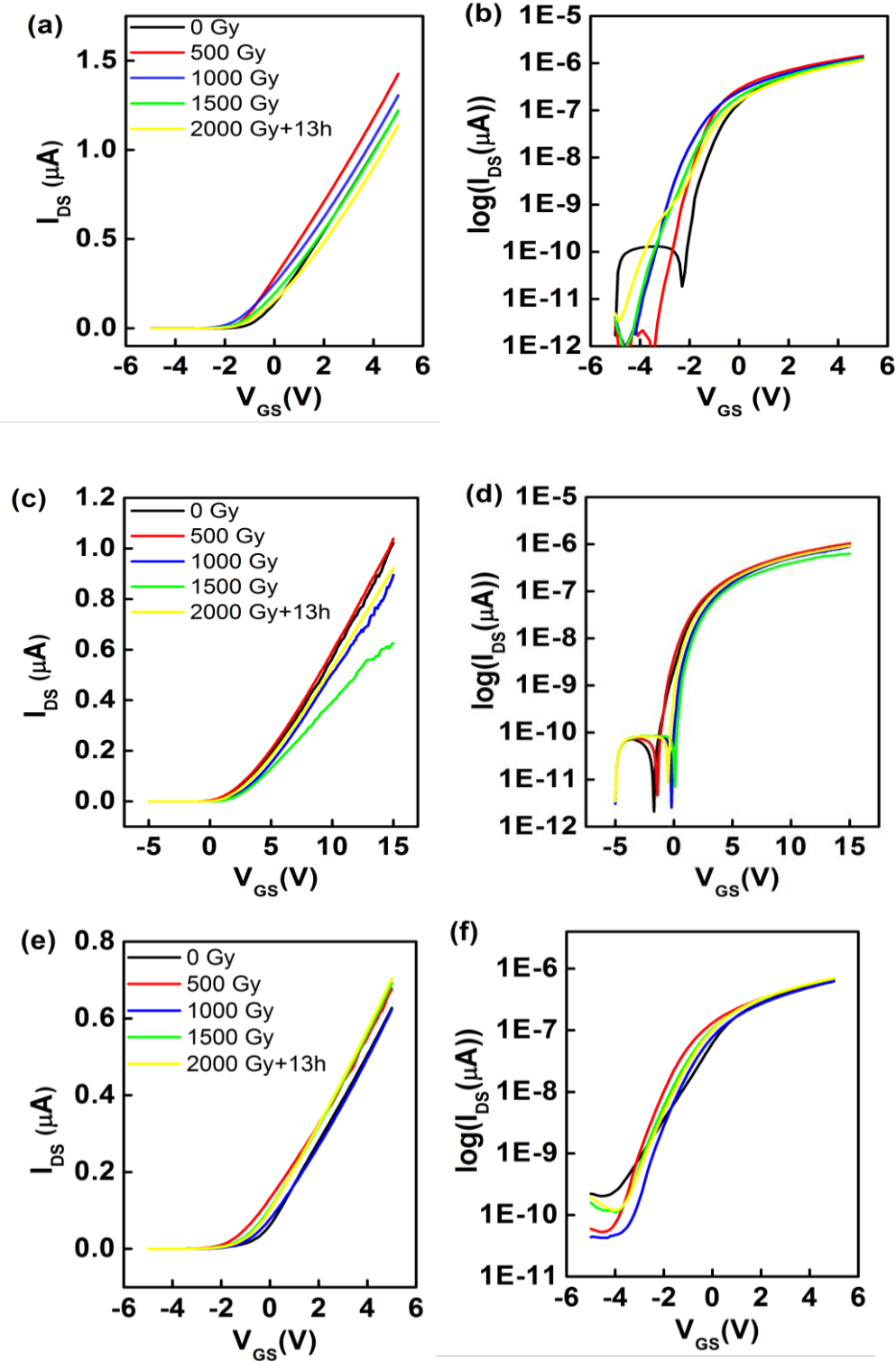
Figure 3.3 – Linear transfer characteristics (VDS=0.1V) on the left (a), (c), (e) and the respective log-scale on the right (b), (d), (f) for oxide TFTs irradiated, each line corresponds to a different dose. The plots (a) and (b) correspond to sample A, (c) and (d) to sample B, and plots (e) and (f) to sample C.

After the first dose applied, 500 *Gy*, it is observed a shift toward negative voltages for all the devices. This shift shows a change in threshold voltage and in subthreshold slope, and it is related with the radiation induced electron-hole pairs and the consecutive build-up charge, which leads to degradation in devices performance. However, just after the first dose applied, the devices

show small changes in their performance as the total dose increased. In the conductive regions of the samples, for V_{GS} higher than 0V (A or C) or 5V (B), an almost overlap of the transfer curves respectively to the doses applied can be observed, suggesting that no significant radiation damage had occurred. Even more, all the samples were able to almost full recover on time as suggested with the plots corresponding to the measurements performed after 13 hours of rest storage on dark. In **Figure 3.3** (a) the recover line overlaps the pristine line for GIZO device, suggesting a total recovery. The pristine line for the ZTO devices, (c) and (e), is almost overlapped by the recover line indicating a partial recovery. Even if it is small changes, remains with a small shift to negative voltages, confirming that trap charges are generated and take time to dynamic anneal process occur. These shifts are in agreement with the ionization damage mechanism [43]. Additionally, to achieve a better analysis of radiation effects, the radiation damage rates were determined estimating a worst case scenario of transistor degradation in a detector electronics. All the results were acquired from statistical analysis, by performing measurements on several TFTs of each sample, calculating the largest possible damage rates which still fall in the 95% confidence interval of the damage rate data. **Figure 3.4** reports the best linear fit, through the parameters extracted from the linear transfer characteristics, of the results with the respective Root Mean Square (RMS) values as a function of cumulative dose for all the samples. RMS values are represented by error bars and the slopes provide the damage rates which describe the change in TFT performance per dose in kGy.
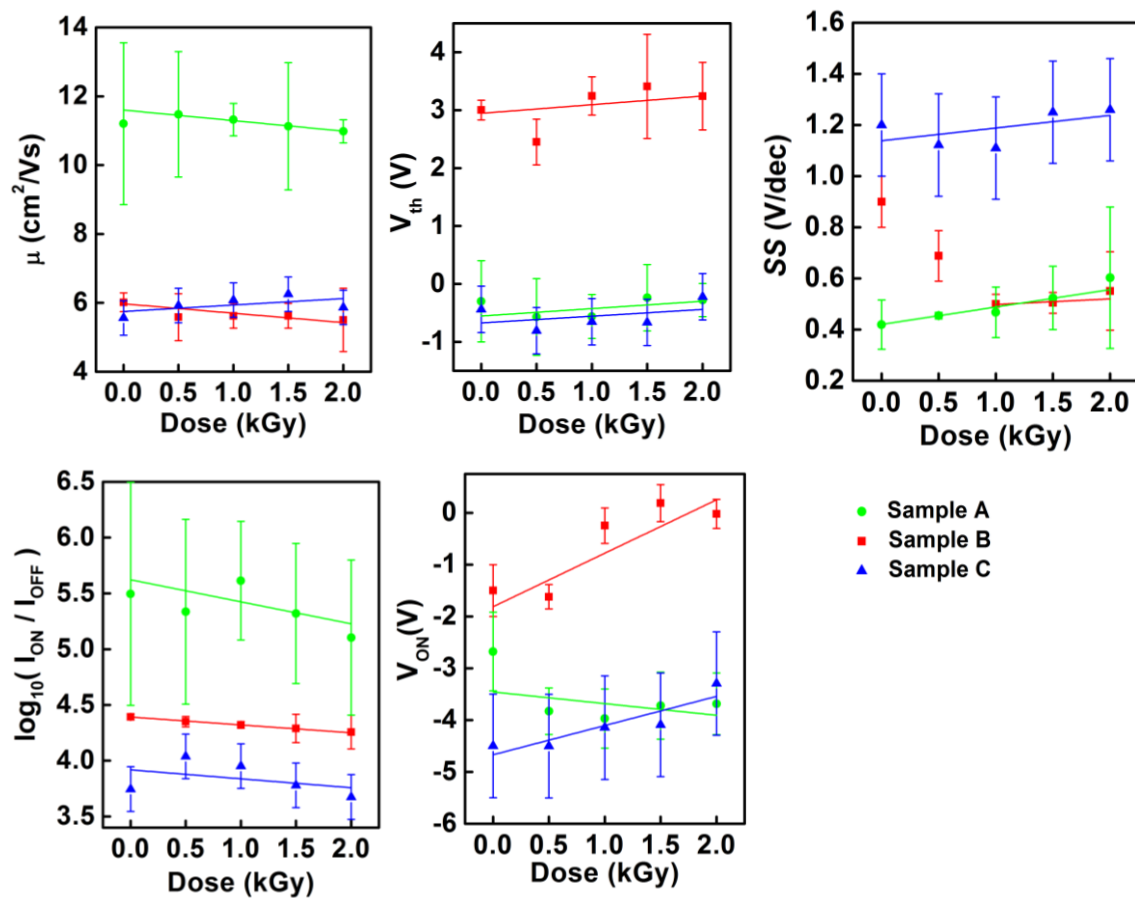

Figure 3.4 – TFTs parameters measured in linear regime (V_{DS} = 0.1 V) as a function of radiation dose.

As already noted above, the irradiation damage is small. All parameters analyzed were affected for all TFTs with the accumulation dose, although the devices show a small changes. For all samples V_{th} increases slightly and the log ratio I_{ON}/I_{OFF} decreases. V_{on} rises accordingly in devices B and C but A shows a slight decrease. In relation to *SS* with cumulative dose, it increases significantly for samples A and C. Sample B shows a particular behavior in which initially *SS* is large, then decreases during the first irradiation interval and finally starts to increase with radiation. Here, we exclude the first two points of sample B from the analysis as the measured values exceed clearly the *SS* values reported for these oxide transistors in literature [31]. The increase on SS and V_{th} was expected due to charge trapping induced by X-rays, which are reported on the shift on transfer characteristics, due to the fixed positive charges and the defects states creation near the interface dielectric/semiconductor.

In **Table 3.2** is documented the values calculated from the linear fits, showing X-rays induced damage rates of TFTs parameters. The confidence interval allows us also to give an upper limit for the maximum observable effect as a worst case scenario for radiation damage.

Table 3.2 – Parameters calculated from linear fits, to determine X-rays induced damage rates of TFTs parameters, are shown in **Figure 3.4**. The upper limit reports the highest possible damage rate within the 95% confidence interval as deduced from the linear fitting procedure.

	Sample A		Sample B		Sample C	
Semiconductor	GIZO		ZTO		ZTO	
Dielectric	Ta2O5/SiO2		SiO2		Ta2O5/SiO2	
Substrate	Glass		Si		Glass	
TFT parameter	**best fit**	**upper limit**	**best fit**	**upper limit**	**best fit**	**upper limit**
$\Delta\mu/\mu_0/\Delta D$ (% kGy^{-1})	-2.8	-4.3	-4.5	-8.4	3.3	12.1
$\Delta V_{th}/\Delta D$ (V kGy^{-1})	0.13	0.44	0.29	0.98	0.12	0.61
$\Delta\log_{10}(I_{on}/I_{off})/\Delta D$ (dec kGy^{-1})	-0.20	-0.64	-0.07	-0.08	-0.08	-0.40
$\Delta SS/\Delta D$ (V dec^{-1} kGy^{-1})	-0.010	0.109	0.068	0.081	0.050	0.105
$\Delta N_t/\Delta D$ (cm^{-2}eV^{-1} kGy^{-1})	2.6×10^{10}	2.4×10^{11}	2.5×10^{11}	3.0×10^{11}	2.7×10^{11}	5.7×10^{11}

The reported mobility changes fall in the range of a few percent per *kGy* and the shifts of characteristic voltages (V_{th}) fall in the range of a few hundred *mV* per *kGy*. Changes in sub-threshold slope *SS* cannot be compared directly between the devices. By using equation (3) we calculate the increase in trap density N_t as a consequence of radiation. The best-fit values are in the range of $\Delta N_t/\Delta D = 2.6 \times 10^{10}$ cm^{-2}eV^{-1}kGy^{-1} for GIZO with Ta$_2$O$_5$/SiO$_2$ based devices. Comparing all these different combination of samples, the worst case scenario predicts changes in device performance which are below 5%/kGy for mobility and voltage shifts are smaller than 1*V*. A comparison between the upper limits for radiation damage rates of the three samples suggests that sample A is the most radiation hard TFT with the lowest risk to have large changes in its parameters.

3.1.2 Organic Thin-Film Transistors

N-type (with Polyera Active Ink) and P-type (TIPS-pentacene) OTFTs were tested, with CYTOP as the dielectric layer all integrated into a PEN substrate. In **Figure 3.5**, it is shown the cross-section schemes from OTFTs.
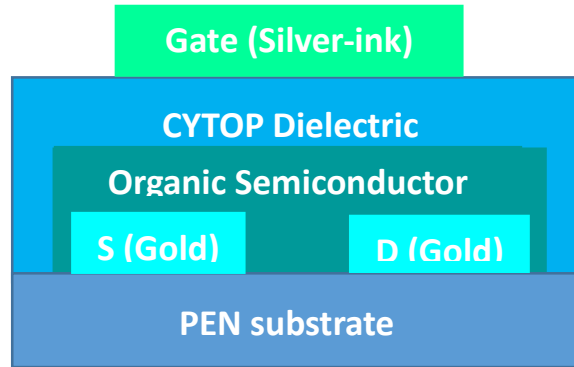
Figure 3.5 – Schematics of the organic TFT cross-sections analysed during this project.

In **Figure 3.6**, it is shown IV measurements done before, during and after X-ray irradiation for N-type. From these (IV and It) measurements, no significant difference was found between measurements with ON and OFF X-rays.
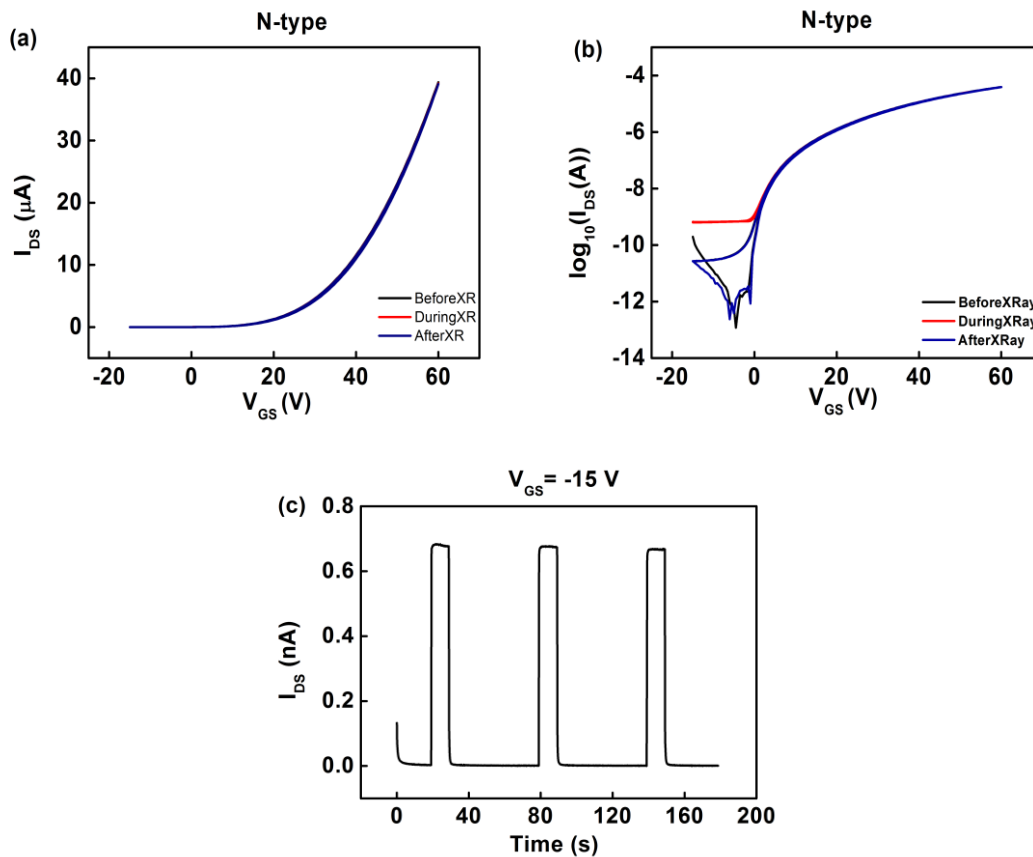
Figure 3.6 – Transfer curves **(a)**, **(b)** N-type (V_{DS} = 60). Before, during x-rays impinging and after x-rays on; **(c)** ON-OFF X-rays with a bias of -15 V for N-type.

As we can verify there are no changes with the ionizing radiation while is impinging on N-type devices, also this was found for P-type. The observed x-ray signal is in the range of typical background photocurrent signal (< 0.5 nA). This indicates, that the organic semiconductor is not significantly affected by X-ray photons on short time scales. No indication for charge carrier formation could be found. From these results we conclude that they are not suitable as detectors.

In addition, similar doses as applied on oxide TFTs were used here to observe some possible changes. Once it is known that organic materials degrade easier than inorganic materials, we decided to investigate how different was the device performance after the first irradiation dose. As an example of the observed effects, **Figure 3.7** reports the transfer characteristics obtained right before irradiation and immediately after exposure of 250 Gy of X-ray to the devices. Also, this figure reports an additional 22 hours of storage in dark. In the pristine state the N-type OTFTs exhibited the following transistor metrics: μ = 0.2 cm^{2}V^{-1}s^{-1}; Vth = 15.4 V; SS = 3.8 V/dec; I$_{OFF}$ = 2 pA. Whereas, for P-type devices: μ = 1.5 cm^{2}V^{-1}s^{-1}; V$_{th}$ = -13.8 V; SS = 4.3 V/dec; I$_{OFF}$ = 0.5 nA.
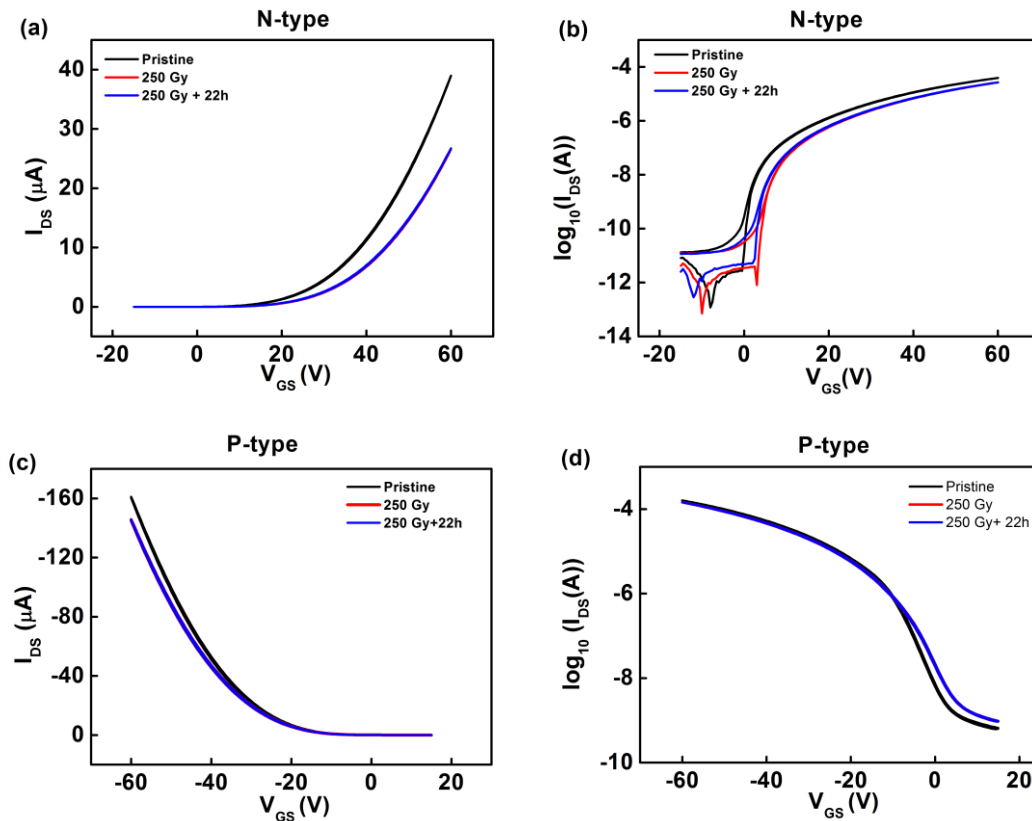
Figure 3.7 – Degradation of transfer characteristics after exposure to 250 Gy of ionizing radiation for n-type and p-type printed organic field effect transistors. Transfer curves acquired in saturation regime **(a), (b)** N-type (V$_{DS}$= 60 V); **(c), (d)** P-type (V$_{DS}$= -60 V).

Exposure to X-ray causes for both kinds of transistors a shift of the transfer curve to positive and negative voltages (N- and P-type OTFTs, respectively), a reduction in mobility and for the P-type device also an increase in subthreshold slope. This degradation is fully preserved during storage in dark at room temperature as demonstrated by the overlap of the transfer curves. The radiation–

induced degradation processes in organic materials are related with the higher sensitivity to the ionizing radiation than other materials, such as metals, which represents a practical problem. In fact, the thermodynamically instability of the covalent bonds in organic semiconductors and the ionization of the material semiconductor chains due to their interaction with high photons energy, are known to lead to the degradation processes, and consequently to the material fragmentation and generation of free radicals. Therefore a permanent damage on OTFTs was found.

In order to investigate the transistor parameters as a function of exposure to ionizing radiation we repeated exposure to 250 Gy and subsequent characterization for four times. The experiment was repeated on different n-type as well as p-type transistors with varying channel geometry (W = 2000 μm; L = 50 μm or 20 μm). In the analysis we averaged the obtained data to calculate statistical variations in the observed damage. As mobilities show already variations between different devices we normalize their values prior to averaging. **Figure 3.8** shows the results from the damage dose rates of organics, mobility normalized indicates a decrease for both type of transistors, showing a higher degradation for N-type. In both cases strong reduction in mobility is observed which follows an exponential decay. This effect is possible related with degradation process which influences on atomic structure, such as polymer chains-scission. Regarding voltage shifts, varation is pratically the same, while subthreshold slope and ON/OFF ratio record larger changes.
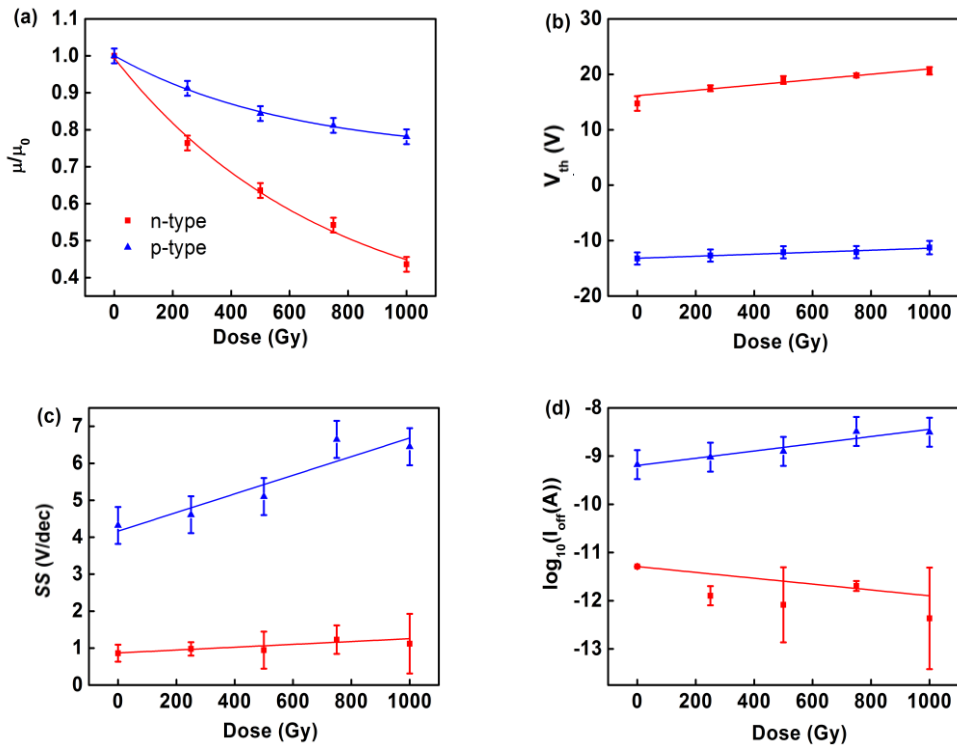

Figure 3.8 – Radiation damage in printed organic thin film transistors. Transistor parameters extracted from transfer curves measured in saturation regime for P- and N-type transistors after exposure to incremental doses of X-ray. **(a)** normalized mobility μ/μ0; **(b)** threshold voltage V_{th}; **(c)** off-current I_{OFF} and **(d)** sub-threshold slope SS.

From the damage dose rates of organics, normalized mobility indicates a decrease for both type of transistors, showing a higher degradation for N-type. In both cases strong reduction in mobility is observed which follows an exponential decay. This effect is possibly related with degradation process which influences on atomic structure, such as polymer chains-scission. Regarding voltage shifts, variation is practically the same, while subthreshold slope and ON/OFF ratio recorded larger changes. **Table 3.3** contains corresponding damage rates obtained from fitting the data.

Table 3.3 – X-ray induced damage rates of transistor parameters mobility µ, threshold voltage Vth and sub-threshold slope SS in n-type and p-type printed OTFTs.

TFT parameter	N-type		P-type	
	best fit	upper limit	best fit	upper limit
$\Delta\mu/\mu_0/\Delta D$ (% kGy-1)	7.30×10^1	1.20×10^1	3.10×10^1	2.30×10^0
$\Delta Vt/\Delta D$ (V kGy-1)	4.8	0.73	1.81	0.24
$\Delta \log_{10}(I_{ON}/I_{OFF})/\Delta D$ (dec kGy-1)	(-0.6)	0.19	0.75	0.13
$\Delta SS/\Delta D$ (V dec-1 kGy-1)	0.38	0.1	2.52	0.55
$\Delta N_t/\Delta D$ (cm-2eV-1 kGy-1)	8.25×10^{10}	2.17×10^{10}	5.5×10^{11}	1.19×10^{11}

For n-type transistors the initial mobility decay rate amounts to 73 %/kGy. The p-type transistors are more stable and mobility decays at 31 %/kGy. For both devices an increase in threshold is observed which is more pronounced for the n-type transistors and amounts to 5V/kGy. The subthreshold voltage remains reasonably stable for N-type devices but P-type devices show an increase of 2.6V/kGy.

In brief, these results indicate several different damages caused by ionizing radiation in these transistors. The shift in threshold voltage to positive voltages in N- as well as P-type devices is attributed to a negative charging of the polymer dielectric caused by the ionizing radiation. Degradation of mobility instead depends on details of the molecular structure of the semiconductor and hence differences in damage rates between N- and P-type molecules are reasonable. The large increase in sub-threshold slope is an interfacial phenomena. Charges which are created by the ionizing radiation are creating additional shallow trap states in the p-type material.

Comparing HMSO-TFTs with OTFTs the radiation stability experiments demonstrate a clear difference between the two kinds of devices. While deterioration of electronic properties has been observed in organic transistors leading to a reduction in mobility of 73% per kilo gray of exposure, no significant adverse effects could be identified in oxide based transistors even when subjected to total doses reaching two kilo gray. Variations in mobility remained below 5% per kilo gray of exposure and changes in operation voltages remained below 200 mV. The only significant effect

is a temporary shift in threshold voltage due to positive charging of the oxide dielectric. The main difference relays on the bonding atomic nature, conjugated polymers present lower carrier mobility, more degradable and inferior radiation tolerance, when compared to silicon, for example. Therefore, the main difference between these two technologies relies on the permanent damage found on OTFTs.

3.2   Organic Semiconducting Single Crystal as detector

In this subsection are presented results on the sensor units performance as X-ray direct detectors. Their performance was determined in terms of the sensitivity, S (nC/Gy), to ionizing X-ray radiation, which is given by equation (4).

$$S = \frac{\Delta I\ (nA)}{D\ (mGy/s)} \tag{4}$$

Where ΔI is the maximum photocurrent signal ($\Delta I = I_{ON} - I_{OFF}$) and D corresponds to the X-rays dose rate. The capability of producing a usable signal for a given type of radiation and energy, in a detector is called sensitivity. Also, for device performance stability and repeatability are important parameters. An interdigitated gold electrodes structure covered by polycrystalline TIPS-pentacene film was tested, investigating the performance after some months without being used and assessing its radiation hardness through X-ray induced degradation processes in the sensor performance. This device have been operated in air at room temperature (RT), at 0.2 V. **Figure 3.9** shows an example of a typical photoresponse of the pristine device performance, for 60 s with X-ray ON with different dose rates applied. The photocurrent can be divided in two parts: first a slow charge; right after X-ray turned ON, a slow building in the photocurrent during all the exposure to radiation, which indicates a progressive creation of photo-generated carriers. Second it is followed by a slow discharge, which is related with traps in the crystals.
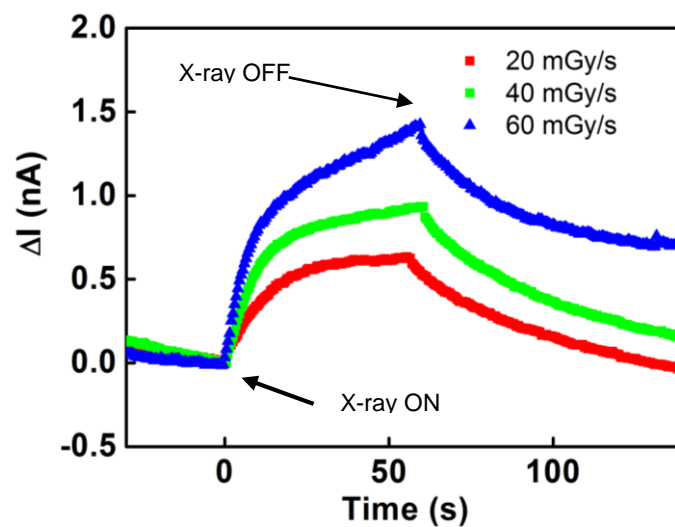

Figure 3.9 – Typical current increase due to X-ray induced carrier generation and subsequent recombination for three different dose rates.

In the earliest study by *Fowler* [9] also this photoresponse has been found for polystyrene polymer as it is possible to verify in **Figure 3.10**, and a schematic illustrating the conductivity induced process. The phenomenon, the slow answer of these devices to X-rays, is related to presence of traps, but the nature of these traps is still unknown [17].
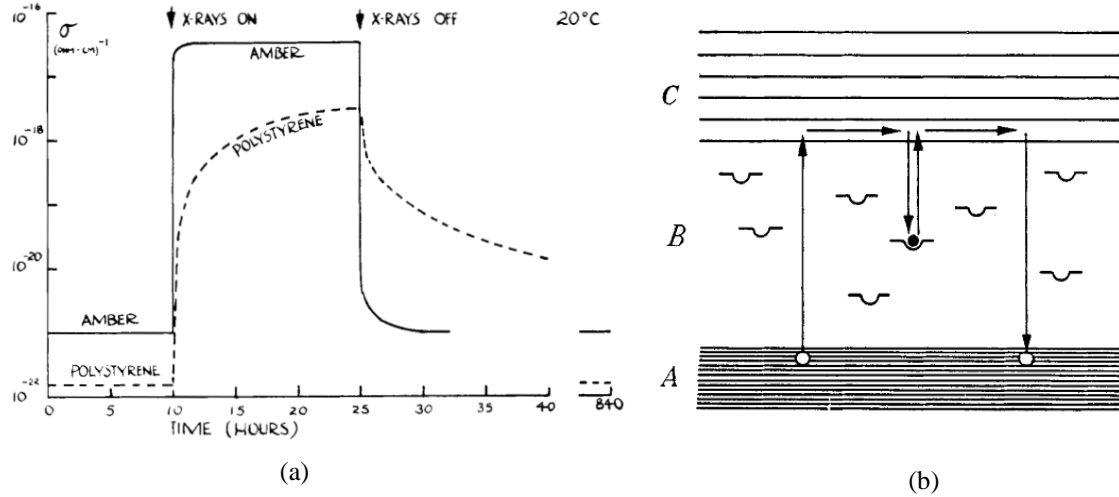

(a)   (b)

Figure 3.10 – (a) Conductivity induced in Amber and polystyrene in function of time; **(b)** Energy level diagram for crystals or single groups of atoms in insulating material [9].

It is preferred the fast photoresponse, the slow TIPS response is a drawback that it is wished to avoid. However, presently, TIPS-pentacene are used because its sensitivity is higher than the other organic single crystals. The sample has been electrical characterized four times at different doses rates with filament currents of 5, 10,15,20,25 and 30 mA, right after being irradiated with a dose rate of 60.4 mGy/s for 70 min. In order to determinate the sensitivity, ΔI values from X-ray induced photocurrent signal were calculated and plotted as function of dose rates, as is present in **Figure 3.11**. Sensitivity is obtained by applying a linear fit to the plot ΔI vs Dose rates. Even more, **Figure 3.11** also reports the current-voltage curves for the increase of doses applied, indicating that as irradiation doses increase the sample becomes more conductive. Also, it is noted an overlap between the pristine measurement and the last measure done after one week storage at room-temperature, which suggests a recover of the crystal.
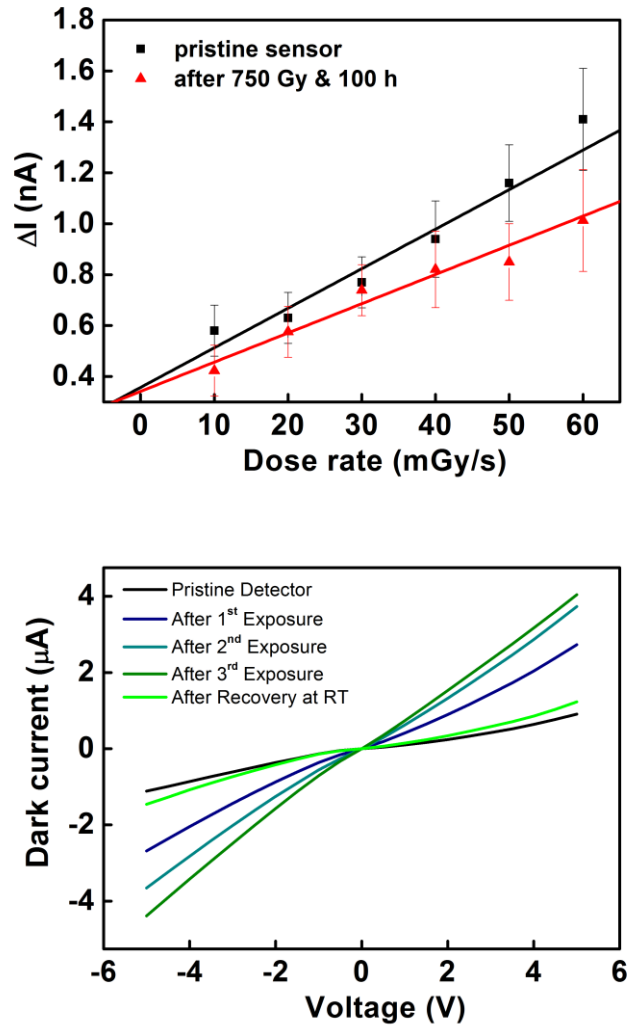
Figure 3.11 – (a) Plot of crystal response with the increasing dose rates biased at 0.2 V, from where sensitivity is extracted, of direct X-ray detection before and after high dose X-ray exposure; **(b)** IV curves acquired in dark after different exposure doses and after recovery with time.

The detector sensitivity before irradiation is 16.9 nC/Gy but after a first dose we observe a big change in the current, which become lower and after one week, the sample recovers partially with a sensitivity of 11 nC/Gy. **Figure 3.12** shows a quantitative analysis of dark current and carrier generation as a function of dose exposure. Both properties deteriorate as a function of irradiation dose. However, also in this case the storage in dark allows recovery of the initial performance and only slightly reduced sensitivity values are obtained after 750 Gy of X-ray exposure and sufficient recovery time.

Figure 3.12 – Maximum X-ray induced current increase during sensing and sensor dark current as a function of exposure dose.

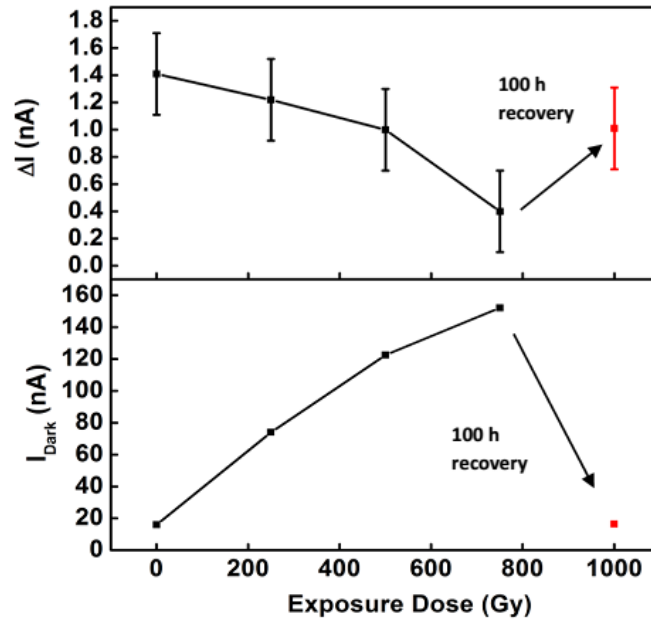After the fourth irradiation step applied to the device is no more able to perform well and it is not possible to extract the sensitivity, due to the deterioration caused by the accumulation of charges. Most notable there is an increase in dark current. Interestingly, if the device is stored in dark at RT, its original properties recover even if the device has been subjected to doses of up to 750 Gy. In addition, it is presented the dynamic electrical response after all doses applied and recover after 100 h, with four cycles switching ON-OFF X-ray at different filament currents in **Figure 3.13**. In summary, first, the exposure to high doses of ionizing radiation deteriorates temporarily the sensibility of the sensor as it decreases with the increase of radiation dose and is not possible to calculate the S, since it is not possible to determine the maximum photocurrent response in some steps. Although, this pristine sensor shows linear response with increasing dose rate, achieving exceptionally high sensitivities. After irradiation the sensor returns to its ground state with a slower dynamics. It is possible to confirm that the sample works as a direct detector, since absorbs X-rays and convert it into electrical signal.
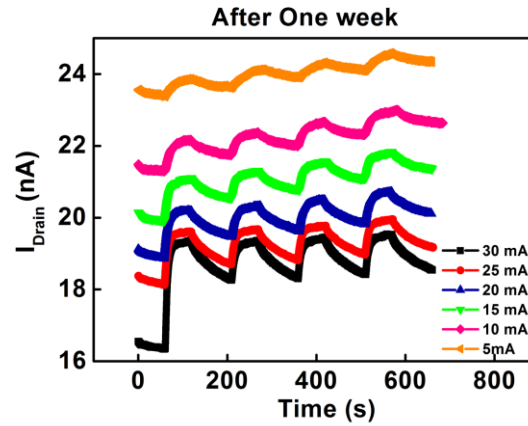
Figure 3.13 – Photo-response as function of the time with the accumulation of radiation recovery after one week of applied last dose.

Relative to **OSSCs fabricated by inkjet, drop-cast:** A diverse set of samples with TIPS-pentacene varying the solvents and their quantity was tested to investigate if they work as detectors. Two results obtained for such samples will be discussed: sample A is composed by 20mg/l of toluene and sample B was made of 20mg/l of tetralin. Their structure presents a coffee-ring structure as shown in **Figure 3.14.** The area inside the coffee-ring is covered by micro/nano-crystalline film.
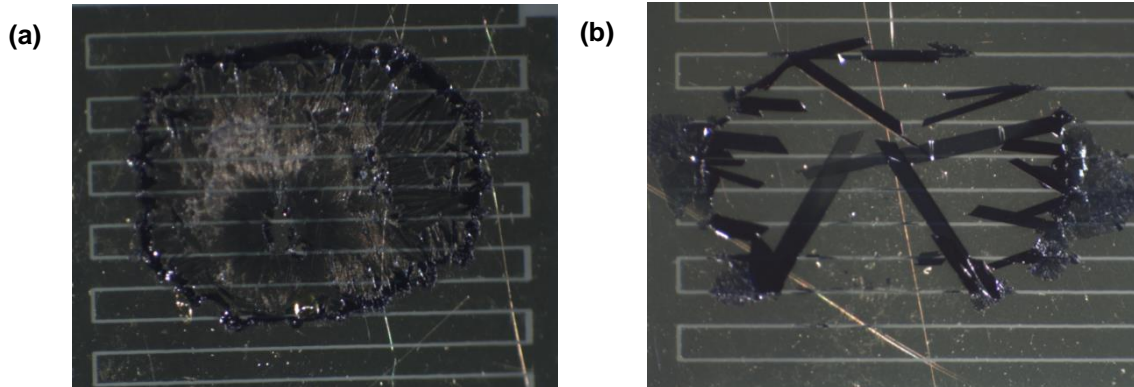
Figure 3.14 – Coffee-ring structure of devices image obtain by Optical Microscopy. **(a)** Sample A, where crystallites with dimensions in the range of 200 μm x 100 μm x 1.5 μm can be found. In the center, surrounded by coffee-ring there is a micro/nano-crystalline film. Typical dimensions of crystallites are 100 μm x 30 μm x 0.3 μm; **(b)** Sample B: formation of larger crystals with thicknesses in the range of 1.8 μm up to 8 μm is visible.

The first measurements with this set of samples were IV measurements taken with a bias voltage range of -5 to 5 V and for -20 and 20 V. **Figure 3.15** shows IV characteristics for samples A and B, which allow to evaluate the dark current behaviour and their conductivity, which follow Schottky-like behavior. Due to so low response in sample B, we decided to anneal and verify any changes. After annealing at 60ºC, measurements were acquired and samples were tested again to see if there were any improvements in the detector performance. Annealing can lead to a more ohmic behavior, as show in **Figure 3.15**.
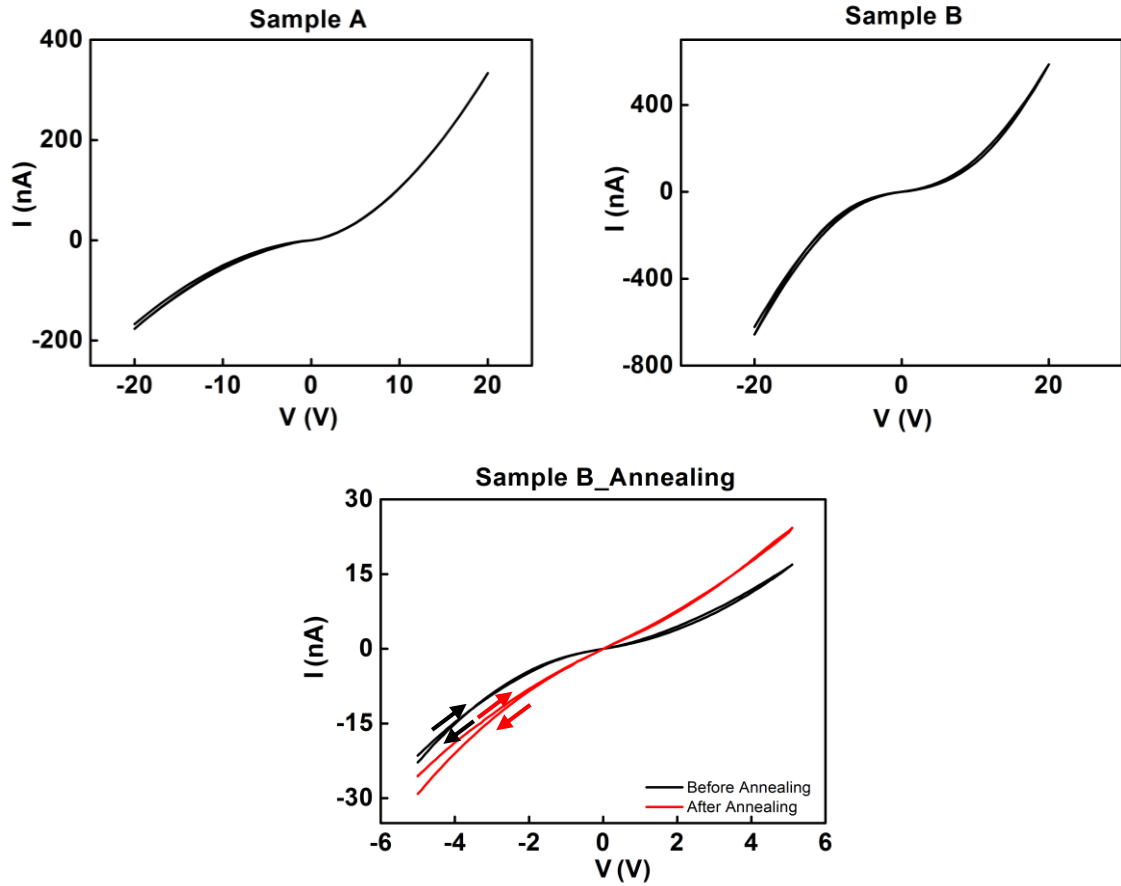
Figure 3.15 – Current-voltage curves for sample A on the left, for sample B on the right and for sample B with 60⁰ of annealing for 30 min, below in the middle.

An enhancement on the conductivity of the sample after annealing and a lower dark current can be observed. Following, current-time measurements were carried out and it is reported the X-ray induced photoresponse recorded by applying 1V and 5V and in **Table 3.4** are reported the photoresponses of the crystals to X-ray for sample A and B after annealing, with three cycles, with X-ray ON for 60s.

Table 3.4 – Maximum photocurrent values obtained for the maximum filament current.

	ΔI (nA)		
	A	**B**	**B annealed**
1V	11.3	0.27	0.31
5V	4.8	0.31	0.67

Figure 3.16 – Sensitivity extracted from the photocurrent response to x-rays by applying 1V: in top sample A; in bottom sample B after annealing at 60⁰. B reports sensitives that exceeds 100 nC/Gy**.**

Lower sensitivities for sample B than for A were recorded. For these samples, the response is slow comparative to other OSSCs based on different organic materials as reported in literature

[5]. It is possible to conclude that TIPS-pentacene responds to X-ray radiation for a dose rate of 60.4 mGy/s. For sample 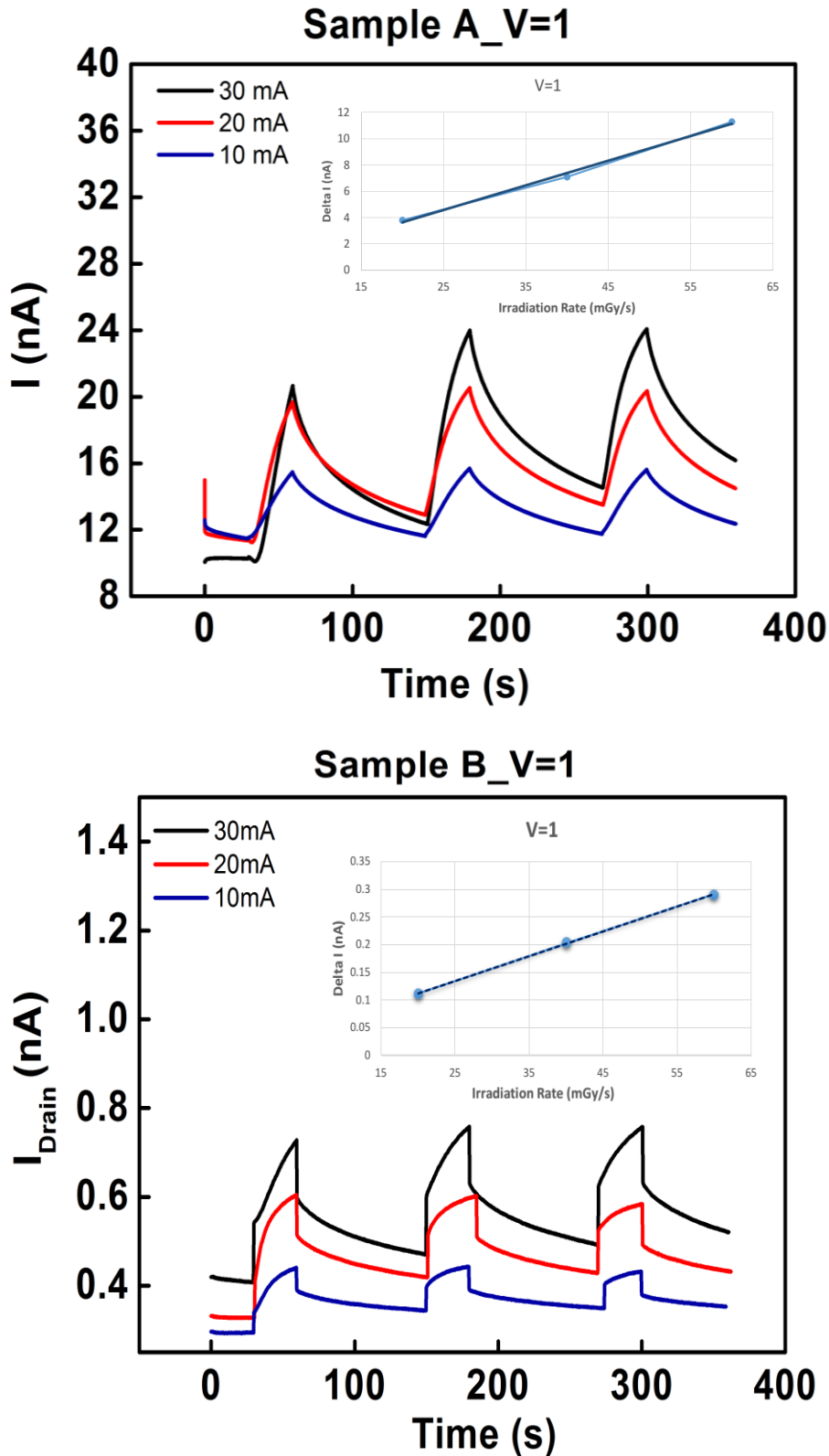A a higher sensitivity is achieved for bias of 5 V, and the sample B has a very low signal (below 1.5 nA). **Table 3.5** shows the sensitivity for these samples.

Table 3.5— Sensitivity values extracted from x-ray photoresponse plots.

	S(nC/Gy)	
	A	**B annealed**
1V	187	4.5
5V	110	14

Comparing these two samples, the ones based on crystals grown using toluene shown a significant response, better detection, achieving sensitivities higher than 100 nC/Gy, although it is important to notice that coffee-ring structure turns difficult the understanding of what is actually the active layer of the sensor, in other words, not only the crystals contribute for X-ray detection but the structure (coffee-ring) that is formed after the material deposition can contribute for the high detection of the device.

These differences in sensitivity values might be related with the size of crystals present in each sample. Also, the high sensitivity of the sample A can be related with the coffee-ring morphology, of the active layer. Even, there were problems in getting reproducible of the results, probably because there was not precise control on the size of the crystals by this method. In addition, crystals sizes are not well controllable as we can see by optical images, the set of samples had more than one device of the same kind (e.g. same solvents, same quantity) and it was difficult to achieve the same photoresponse in the sample, which means that reproducibility and stability of the photoresponse in the sample kind of sample are still issues to overcome.

In summary, the annealing resulted in a small increase on the sensitivity and the choice of the solvent for TIPS-Pentacene influences the crystals growth, and consequently crystals sizes play an important part in the detection capability of the sensor.

Chapter 4 Conclusions and Future Perspectives

In this thesis radiation hardness of the main building-blocks of the i-Flexis X-ray detection system have been investigated. In one hand, the building blocks include TFTs to realize detector backplane electronics and signal amplification electronics. Due to requirements of low-cost, large area and flexibility, TFTs are based on HMSO or organic semiconductors. On the other hand the i-Flexis system relies on direct X-ray photoconverters made of organic semiconducting crystals.

The TFT characteristics show little variation as a function of total ionizing dose and losses in mobility remain in the range of a few percent per kGy. In conclusion, HMSO-TFTs were identified as a suitable main building block for radiation hard and degradation resistant electronics. They can be employed as switches in the pixel arrays of real-time X-ray detectors, whose electronics is directly exposed to the irradiating beam. In contrast, printed OTFTs demonstrated good stability towards normal storage conditions, but suffered degradation upon X-ray exposure which led to a strong reduction in carrier mobility. As a result these devices are not suitable in radiation harsh environments.

Direct X-ray detectors based on organic micro-crystalline films of TIPS-pentacene were evaluated in the degradation experiments. These detectors show good storage stability and reasonable X-ray sensitivity was found even after months of storage. Exposition of the detectors to large total doses at high dose rates leads to deterioration of detector properties such as an increase in dark-current and reduction in sensitivity. However, detector properties recover, when stored in dark at room temperature. Thus damage is reversible and we conclude that the organic detectors are radiation hard for low-dose rate applications (such as medical imaging where total doses are accumulated over a year of operation time). Microcrystalline films show an exceptionally strong response, but scaling the response to the actual area covered by the semiconductor shows that larger semiconducting crystals are likely to be more sensitive. As a general goal we identify to improve repeatability and to reduce the dark current in the tested detectors. Further investigations are needed to understand in detail the temporary radiation damage and its recovery in organic detectors. In addition, further efforts are needed to identify the best performing organic single crystals for direct X-ray detection.

Bibliography

[1]   A. Intaniwet, C. A. Mills, M. Shkunov, H. Thiem, J. L. Keddie, and P. J. Sellin, "Characterization of thick film poly(triarylamine) semiconductor diodes for direct x-ray detection," *J. Appl. Phys.*, vol. 106, no. 6, pp. 1–7, 2009.

[2]   B. Fraboni, A. Ciavatti, L. Basiricò, and A. Fraleoni-Morgera, "FD 174: Organic semiconducting single crystals as solid-state sensors for ionizing radiation," *Faraday Discuss.*, pp. 1–16, 2014.

[3]   R. A. Street, "Thin-film transistors," *Adv. Mater.*, vol. 21, no. 20, pp. 2007–2022, 2009.

[4]   B. Fraboni and A. Fraleoni-morgera, "Organic Semiconducting Single Crystals as Novel Room-Temperature, Low-Cost Solid-State Direct X-Ray Detectors, Solid-State Radiation Detectors: Technology and Applications," Salah Awadalla, Ed. 2014, pp. 243–260.

[5]   B. Fraboni, A. Ciavatti, F. Merlo, L. Pasquini, A. Cavallini, A. Quaranta, A. Bonfiglio, and A. Fraleoni-Morgera, "Organic semiconducting single crystals as next generation of low-cost, room-temperature electrical X-ray detectors," *Adv. Mater.*, vol. 24, no. 17, pp. 2289–2293, May 2012.

[6]   V. I. Mikla and V. V. Mikla, "X-Ray Detectors," in *Medical Imaging Technology*, 2014, pp. 65–87.

[7]   A. Intaniwet, C. Mills, M. Shkunov, P. Sellin, and J. Keddie, "Heavy metallic oxide nanoparticles for enhanced sensitivity in semiconducting polymer x-ray detectors," *IOP Sci.*, vol. 23, pp. 1–7, 2012.

[8]   F. A. Boroumand, M. Zhu, A. B. Dalton, J. L. Keddie, P. J. Sellin, and J. J. Gutierrez, "Direct x-ray detection with conjugated polymer devices," *Appl. Phys. Lett.*, vol. 91, no. 2007, pp. 2007–2009, 2007.

[9]   J. F. Fowler, "X-Ray Induced Conductivity in Insulating Materials," *Proc. R. Soc. London. Ser. A. Math. Phys. Sci.*, vol. 236, no. 1207, pp. 464–480, 1956.

[10]   G. I. and Y. I. K. Yoshino, S. Hayashi, "Eletrical Transport in Electron Beam Irradiated Polyacetylene," *Solid State Commun.*, vol. 46, no. 5, pp. 389–391, 1983.

[11]   L. Basiricò, A. Ciavatti, M. Sibilia, A. Fraleoni-morgera, S. Trabattoni, and A. Sassella, "Solid State Organic X-Ray Detectors Based on Rubrene Single Crystals," vol. 62, no. 4, pp. 1791–1797, 2015.

[12]   S. K. Park, T. N. Jackson, J. E. Anthony, and D. a. Mourey, "High mobility solution processed 6,13-bis(triisopropyl-silylethynyl) pentacene organic thin film transistors," *Appl. Phys. Lett.*, vol. 91, no. 6, pp. 10–13, 2007.

[13]   G. Murtaza, I. Ahmad, H. Chen, and J. Wu, "Study of 6,13-bis(tri-isopropylsilylethynyl)

pentacene (TIPS-pentacene crystal) based organic field effect transistors (OFETs)," *Synth. Met.*, vol. 194, pp. 146–152, 2014.

[14] G. Murtaza, I. Ahmad, and J. Wu, "A comparison of two crystals of 6,13-bis (tri-isopropylsilylethynyl) pentacene (TIPS-pentacene) prepared for organic field effect transistors (OFETs)," *Solid. State. Electron.*, vol. 109, pp. 76–81, 2015.

[15] H. Klauk, "Organic thin-film transistors.," *Chem. Soc. Rev.*, vol. 39, no. 7, pp. 2643–2666, 2010.

[16] H. Dong, H. Zhu, Q. Meng, X. Gong, and W. Hu, "Organic photoresponse materials and devices," *Chem. Soc. Rev.*, vol. 41, no. 5, p. 1754, 2012.

[17] A. Intaniwet, C. a Mills, P. J. Sellin, M. Shkunov, and J. L. Keddie, "Achieving a stable time response in polymeric radiation sensors under charge injection by X-rays.," *ACS Appl. Mater. Interfaces*, vol. 2, no. 6, pp. 1692–9, 2010.

[18] A. a. Virkar, S. Mannsfeld, Z. Bao, and N. Stingelin, "Organic semiconductor growth and morphology considerations for organic thin-film transistors," *Adv. Mater.*, vol. 22, no. 34, pp. 3857–3875, 2010.

[19] H. Jiang and C. Kloc, "Single-crystal growth of organic semiconductors," *MRS Bull.*, vol. 38, no. 01, pp. 28–33, 2013.

[20] H. Minemawari, T. Yamada, H. Matsui, J. Tsutsumi, S. Haas, R. Chiba, R. Kumai, and T. Hasegawa, "Inkjet printing of single-crystal films.," *Nature*, vol. 475, no. 7356, pp. 364–367, 2011.

[21] A. L. Briseno, S. C. B. Mannsfeld, M. M. Ling, S. Liu, R. J. Tseng, C. Reese, M. E. Roberts, Y. Yang, F. Wudl, and Z. Bao, "Patterning organic single-crystal transistor arrays.," *Nature*, vol. 444, no. 7121, pp. 913–917, 2006.

[22] E. Fortunato, P. Barquinha, and R. Martins, "Oxide semiconductor thin-film transistors: a review of recent advances.," *Adv. Mater.*, vol. 24, no. 22, pp. 2945–86, Jun. 2012.

[23] P. F. Moonen, I. Yakimets, and J. Huskens, "Fabrication of transistors on flexible substrates: from mass-printing to high-resolution alternative lithography strategies.," *Adv. Mater.*, vol. 24, no. 41, pp. 5526–41, Nov. 2012.

[24] T. Sekitani, U. Zschieschang, H. Klauk, and T. Someya, "Flexible organic transistors and circuits with extreme bending stability," *Nat. Mater.*, vol. 9, no. 12, pp. 1015–1022, 2010.

[25] T. Sekitani and T. Someya, "Stretchable, Large-area Organic Electronics," *Adv. Mater.*, vol. 22, no. 20, pp. 2228–2246, 2010.

[26] H. Li, G. Giri, J. B. H. Tok, and Z. Bao, "Toward high-mobility organic field-effect transistors: Control of molecular packing and large-area fabrication of single-crystal-based devices," *MRS Bull.*, vol. 38, no. 01, pp. 34–42, 2013.

[27]   P. Bahubalindruni, B. Silva, V. Tavares, P. Barquinha, N. Cardoso, P. de Oliveira, R. Martins, and E. Fortunato, "Analog Circuits With High-Gain Topologies Using a-GIZO TFTs on Glass," *J. Disp. Technol.*, vol. 11, no. c, pp. 1–1, 2014.

[28]   J. S. Jung, K. H. Lee, K. S. Son, J. S. Park, T. S. Kim, J. H. Seo, J. H. Jeon, M. P. Hong, J. Y. Kwon, B. Koo, and S. Lee, "The Effect of Passivation Layers on the Negative Bias Instability of Ga–In–Zn–O Thin Film Transistors under Illumination," *Electrochem. Solid-State Lett.*, vol. 13, no. 11, p. H376, 2010.

[29]   D. S. Han, Y. J. Kang, J. H. Park, H. T. Jeon, and J. W. Park, "Influence of molybdenum source/drain electrode contact resistance in amorphous zinc–tin-oxide (a-ZTO) thin film transistors," *Mater. Res. Bull.*, vol. 58, pp. 174–177, Oct. 2014.

[30]   Y. S. Rim, D. L. Kim, W. H. Jeong, S. J. Kim, B. S. Kim, and H. J. Kim, "Influence of thermal parameter on solution-processed Zr-doped ZTO thin-film transistors," *Curr. Appl. Phys.*, vol. 11, no. 1 SUPPL., pp. 258–261, 2011.

[31]   P. Barquinha, L. Pereira, G. Gonçalves, D. Kuscer, M. Kosec, A. Vilà, A. Olziersky, J. R. Morante, R. Martins, and E. Fortunato, "Low-temperature sputtered mixtures of high-k and high bandgap dielectrics for GIZO TFTs," *J. Soc. Inf. Disp.*, vol. 18, no. 10, p. 762, 2010.

[32]   W. L. Kalb, T. Mathis, S. Haas, a. F. Stassen, and B. Batlogg, "Organic small molecule field-effect transistors with Cytop gate dielectric: Eliminating gate bias stress effects," *Appl. Phys. Lett.*, vol. 90, no. 9, pp. 2005–2008, 2007.

[33]   G. F. Knoll, "*Radiation Detection and Measurement".*, Wiley, fou. 2011.

[34]   W. R. Leo, "*Techniques for Nuclear and Particle Physics Experiments".* Springer-Verlag, 1987.

[35]   H. Spieler, "Introduction to radiation-resistant semiconductor devices and circuits," *AIP Conf. Proc.*, vol. 390, pp. 23–49, 1997.

[36]   T. R. Oldham and F. B. McLean, "Total ionizing dose effects in MOS oxides and devices," *IEEE Trans. Nucl. Sci.*, vol. 50, no. 3, pp. 483–499, Jun. 2003.

[37]   J. M. Boudry and L. E. Antonuk, "Radiation damage of amorphous silicon, thin-film, field-effect transistors.," *Med. Phys.*, vol. 23, no. 5, pp. 743–754, 1996.

[38]   Y. Li, L. E. Antonuk, Y. El-Mohri, Q. Zhao, H. Du, A. Sawant, and Y. Wang, "Effects of x-ray irradiation on polycrystalline silicon, thin-film transistors," *J. Appl. Phys.*, vol. 99, no. 6, 2006.

[39]   S. C. Grahaml, "The effect of X-ray irradiation on poly (p-phenylene vinylene) and derivatives," vol. 84, pp. 903–904, 1997.

[40]   M. Atreya, S. Li, E. T. Kang, K. G. Neoh, Z. H. Ma, K. L. Tan, and W. Huang, "Stability studies of poly(2-methoxy-5-(2 '-ethyl hexyloxy)-p-(phenylene vinylene) [MEH-PPV]," *Polym. Degrad. Stab.*, vol. 65, no. 2, pp. 287–296, 1999.

[41] E. A. B. Silva, J. F. Borin, P. Nicolucci, C. F. O. Graeff, T. G. Netto, and R. F. Bianchi, "Low dose ionizing radiation detection using conjugated polymers," *Appl. Phys. Lett.*, vol. 86, no. 13, pp. 1–3, 2005.

[42] R. A. Lujan and R. A. Street, "Flexible X-Ray Detector Array Fabricated With Oxide Thin-Film Transistors," *IEEE Electron Device Lett.*, vol. 33, no. 5, pp. 688–690, May 2012.

[43] J. R. Schwank, M. R. Shaneyfelt, D. M. Fleetwood, J. A. Felix, P. E. Dodd, P. Paillet, and V. Ferlet-Cavrois, "Radiation effects in MOS oxides," *IEEE Trans. Nucl. Sci.*, vol. 55, no. 4, pp. 1833–1853, 2008.
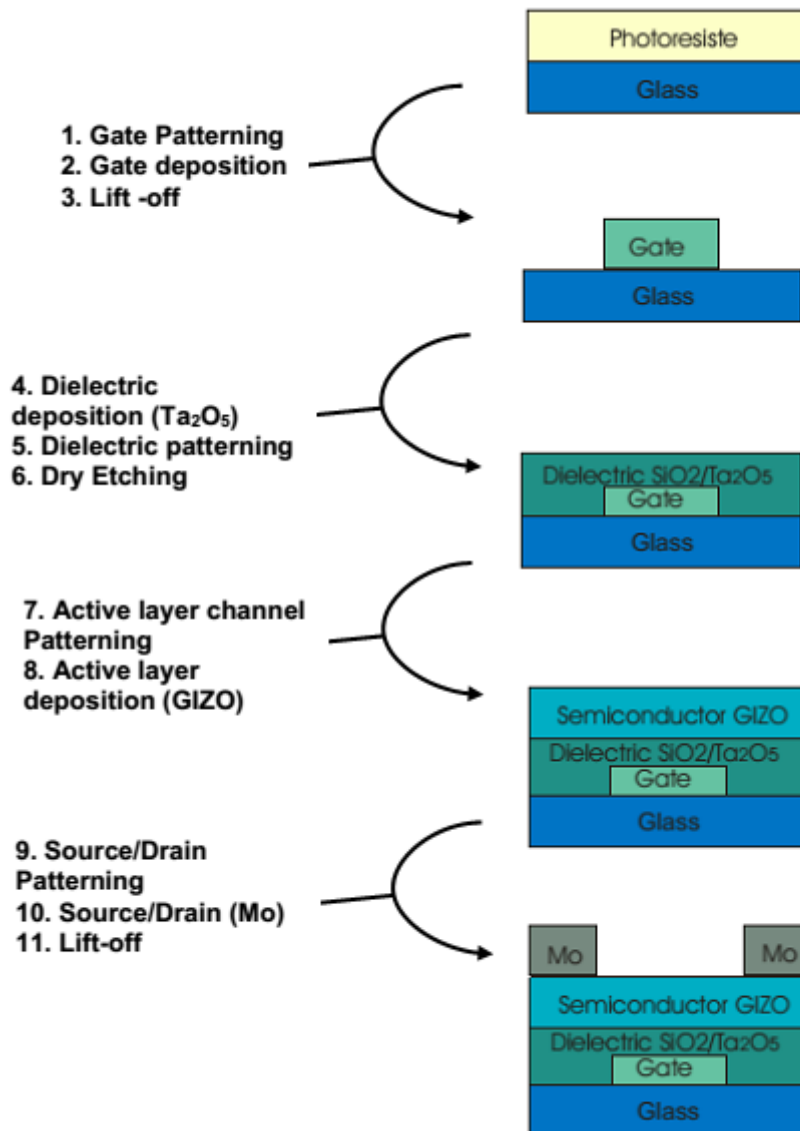
Appendices

Appendix 1

Figure 0.1 – Briefly description of oxide TFTs fabrication employing sputtering and photolithography techniques.

Appendix 2

125 µm PEN foil with 30 nm gold layer

Access lines (columns) and transistors S/D patterning
by photolithography

Semiconductor (P-Type small molecule) deposition
patterned by screen-print

Dielectric (CYTOP-like) deposition
patterned by screen-print

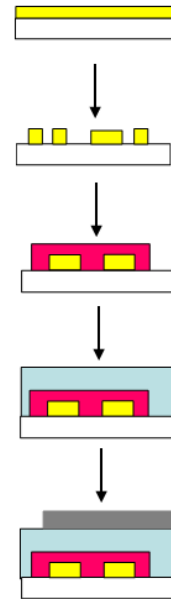Silver access lines (rows) and gate deposition
patterned by screen-print

Figure 0.2 – Characteristics of organic printed OTFT on flexible substrate as developed by CEA:
schematics of device structure.